Received: 12 May 2021 | Revised: 19 August 2021 | Accepted: 19 August 2021

DOI: 10.1111/pce.14177

ORIGINAL ARTICLE

Plant, Cell & Environment WILEY

Drone-based physiological index reveals long-term acclimation and drought stress responses in trees

Petra D'Odorico[1] | Leonie Schönbeck[2,3] | Valentina Vitali[1] | Katrin Meusburger[4] | Marcus Schaub[1] | Christian Ginzler[5] | Roman Zweifel[1] | Vera Marjorie Elauria Velasco[6] | Jonas Gisler[1] | Arthur Gessler[1,7] | Ingo Ensminger[8]

[1]Forest Dynamics Research Unit, Swiss Federal Institute for Forest, Snow and Landscape Research WSL, Birmensdorf, Switzerland

[2]Plant Ecology Research Laboratory, School of Architecture, Civil and Environmental Engineering, EPFL, Lausanne, Switzerland

[3]Community Ecology Unit, Swiss Federal Institute for Forest, Snow and Landscape Research WSL, Lausanne, Switzerland

[4]Biogeochemistry Unit, Swiss Federal Institute for Forest, Snow and Landscape Research WSL, Birmensdorf, Switzerland

[5]Land Change Science Unit, Swiss Federal Institute for Forest, Snow and Landscape Research WSL, Birmensdorf, Switzerland

[6]Office of the Vice-Principal Research, University of Toronto Mississauga, Mississauga, Ontario, Canada

[7]Department of Environmental Systems Science, ETH Zürich, Zürich, Switzerland

[8]Department of Biology, University of Toronto Mississauga, Mississauga, Ontario, Canada

Correspondence
Petra D'Odorico, Forest Dynamics Research Unit, Swiss Federal Institute for Forest, Snow and Landscape Research WSL, Zürcherstrasse 111, 8903 Birmensdorf, Switzerland.
Email: petra.dodorico@wsl.ch

Funding information
Swiss National Science Foundation (SNSF), Grant/Award Numbers: CRSK-3_190802, 310030_189109; National Science and Engineering Council (NSERC), Grant/Award Number: RGPIN-2020-06928

Abstract

Monitoring early tree physiological responses to drought is key to understanding progressive impacts of drought on forests and identifying resilient species. We combined drone-based multispectral remote sensing with measurements of tree physiology and environmental parameters over two growing seasons in a 100-y-old *Pinus sylvestris* forest subject to 17-y of precipitation manipulation. Our goal was to determine if drone-based photochemical reflectance index (PRI) captures tree drought stress responses and whether responses are affected by long-term acclimation. PRI detects changes in xanthophyll cycle pigment dynamics, which reflect increases in photoprotective non-photochemical quenching activity resulting from drought-induced photosynthesis downregulation. Here, PRI of never-irrigated trees was up to 10 times lower (higher stress) than PRI of irrigated trees. Long-term acclimation to experimental treatment, however, influenced the seasonal relationship between PRI and soil water availability. PRI also captured diurnal decreases in photochemical efficiency, driven by vapour pressure deficit. Interestingly, 5 years after irrigation was stopped for a subset of the irrigated trees, a positive legacy effect persisted, with lower stress responses (higher PRI) compared with never-irrigated trees. This study demonstrates the ability of remotely sensed PRI to scale tree physiological responses to an entire forest and the importance of long-term acclimation in determining current drought stress responses.

KEYWORDS
acclimation, drone, drought stress, evergreen, functional traits, photoprotection, PRI, UAV, xanthophyll cycle pigments

Arthur Gessler and Ingo Ensminger should be considered joint senior authors.

1 | INTRODUCTION

Observed upward trends in global drought over the past decades and model predictions both suggest that the next decades will be characterized by severe and widespread droughts in northern mid to high latitudes, resulting from either decreased precipitation and/or increased evaporation (Dai, 2013). Consequently, many tree species will experience increasingly unfavourable environmental conditions in their current range of distribution (Bussotti, Pollastrini, Holland, & Brüggemann, 2015; Chauvier et al., 2020; Stahl, Reu, & Wirth, 2014; Williams et al., 2013). As sessile organisms with a long lifespan, their fitness and ultimately survival is closely tied to the ability to respond to these climatic changes through the adjustment of key plant traits involved in the avoidance and tolerance of drought stress. Acclimation, through phenotypic plasticity, in these traits can temporarily compensate for the maladaptation until genetic adaptive variation is restored by gene flow and hybridization (Gessler, Bottero, Marshall, & Arend, 2020; Kremer, Potts, & Delzon, 2014; Nicotra et al., 2010).

In the temperate climate zone, summer droughts are typically caused by the co-occurrence of high light intensity, high temperature and water shortage (De Boeck & Verbeeck, 2011). As a result of this condition, trees activate a cascade of physiological responses. Photosynthesis is progressively downregulated, initially through drought-induced stomatal closure, which decreases atmospheric CO_2 uptake by leaves and thus reduces CO_2 availability in the chloroplasts. This, in turn, decreases the amount of light required to saturate photosynthesis, creating an excess of energy that needs to be safely dissipated to avoid severe photoinhibition and photooxidation, which lead to photosystem damage (Flexas & Medrano, 2002).

Plants have developed different protective mechanisms to safely dissipate excess light energy during periods of stress. Among these, thermal dissipation mediated by the xanthophyll cycle was first described by Demmig, Winter, Krüger, and Czygan (1988) and later confirmed to be a flexible and ubiquitous process common to all plant species (Demmig-Adams & Adams, 1996; Demmig-Adams & Adams III, 2006; Flexas & Medrano, 2002; Jahns & Holzwarth, 2012). This mechanism is responsible for dissipating the majority of excess energy during drought, which, according to a meta-analysis by Flexas and Medrano (2002), can amount to 70%–90% of the total light absorbed by C3 plants.

Thermal energy dissipation under excess light is accomplished via a de-epoxidation reaction stimulating the interconversion of xanthophyll cycle pigments, where violaxanthin is converted, via the intermediate antheraxanthin, to zeaxanthin. The inverse epoxidation reaction is triggered by low light (Demmig-Adams & Adams, 1996; Niyogi, 1999). Thus, under drought stress, when the absorption of light by chlorophyll outweighs its utilization through photosynthetic carbon metabolism, zeaxanthin is the predominant xanthophyll cycle pigment found in leaves.

Photoprotection includes mechanisms acting across different temporal scales. The above-described rapid (within minutes) de-epoxidation of the xanthophyll cycle pigments provides flexible non-photochemical quenching (NPQ) of excess light energy, a mechanism that gives insight into the photochemical efficiency of leaves as a direct response to increasing stress. Over long (seasonal) timescales, changes in carotenoid pigment pools, including changes in the total size of the xanthophyll cycle pool (i.e., the sum of violaxanthin + antheraxanthin + zeaxanthin), define the capacity for zeaxanthin formation and thus reflect the investment in photoprotection by leaves (Demmig-Adams & Adams, 1993). The slow or irreversible adjustments in carotenoid pigments pool sizes follow seasonal acclimation to the light environment, rising with increasing degrees of excess light over the season (Demmig-Adams & Adams, 1996).

The ability to assess early (pre-visual) tree physiological responses to stress, like changes in photoprotection, is as important as assessing late physiological and structural effects such as leaf browning and wilting or canopy defoliation, which often represent irreversible damage to the status of plants. Early assessment can lead to an improved understanding and monitoring of the progressive impacts of intensifying droughts on our forests, which can inform the development of mitigation strategies, including the identification of more resilient tree species and genotypes.

Optical remote sensing indices targeting reflectance at wavelengths sensitive to pigment composition and absorption changes provide a unique non-destructive means to obtain insight into plant physiological processes. In particular, the remotely sensed photochemical reflectance index (PRI), which in its classical formulation compares the xanthophyll-induced reflectance change at 531 nm to a xanthophyll-independent reference band at 570 nm, has been proposed as an indicator of plants' light use efficiency and stress responses (Gamon, Peñuelas, & Field, 1992; Gamon, Serrano, & Surfus, 1997). Since PRI measures the relative reflectance on either side of the green reflectance hump (550 nm), it also compares the reflectance in the blue (chlorophyll and carotenoid absorption) region of the spectrum with reflectance in the red (only chlorophyll absorption) region. Thus, PRI also has the ability to track the relative carotenoid/chlorophyll ratio, which is indicative of slow changes in pigment pool sizes over the growing' season (Filella et al., 2009; Wong, D'Odorico, Arain, & Ensminger, 2020). Together, its sensitivity to the de-epoxidation state of the xanthophyll cycle over a short timescale and to carotenoid/chlorophyll pool sizes over a long seasonal time scale ensure that PRI scales with photosynthetic efficiency across a wide range of environmental conditions and plant functional types (Garbulsky, Peñuelas, Gamon, Inoue, & Filella, 2011). While measurements of PRI at the leaf level set the mechanistic basis for its application as a physiological proxy, its full potential for forest monitoring unfolds with the scaling from the leaf to the canopy level. In a past study we demonstrated that leaf PRI derived from proximal spectral measurements successfully scaled to canopy PRI obtained from spectral reflectance sensors mounted on towers above the forest canopy (Wong et al., 2020). Sensors onboard drone platforms, as employed here take the scaling one step further, making it possible to obtain canopy-integrated response values for entire tree populations including thousands of individuals. This gives a more ecologically indicative picture of forest stand conditions, which is relevant for comparisons with regional climate information and supports causal inference.

Dry inner-Alpine valleys, at the transition between continental and Mediterranean climates, have experienced a more frequent occurrence of severe summer droughts followed by a steep increase in tree mortality since the 1990s (Rigling et al., 2013). Characterized by a wide range of distribution explaining its high genetic variation (Tyrmi et al., 2020), *Pinus sylvestris* L. (Scots pine) is known for its pronounced drought tolerance and undemanding nature regarding soil type and water supply (Richardson, 1998). However, there is also evidence of an increased vulnerability of *P. sylvestris* during early recruitment stages (Ramírez-Valiente et al., 2021) and along the southernmost limit of its distribution area in southern Europe (Dorado-Liñán et al., 2019). At the southern edge of its distribution on the lower Alpine slopes in the Swiss canton of Valais, *P. sylvestris* has been declining, with slower growth and an increased probability of mortality correlating with drought years over the last century (Bigler, Bräker, Bugmann, Dobbertin, & Rigling, 2006; Rebetez & Dobbertin, 2004; Rigling et al., 2013).

Taking advantage of a long-term (17-year) precipitation manipulation (irrigation) experiment in a dry inner-Alpine valley in Switzerland and the natural environmental fluctuations during 2 years of measurements, we studied drought responses of a 100-year-old *P. sylvestris* forest. Specifically, we combined datasets from repeated drone-based remotely sensed multispectral imaging with measurements of physiological processes and environmental drivers to (a) determine if a remotely sensed physiological proxy (i.e., drone-based photochemical reflectance index, PRI) can capture differences in the drought and recovery response of mature *P. sylvestris* populations and to what extent it matches leaf-level pigments and physiological measurements; and (b) investigate whether long-term tree acclimation affects the current drought stress response of *P. sylvestris*. We hypothesized that tree responses to atmospheric and soil drought would differ depending on whether trees were acclimated to naturally dry conditions or a favourable water supply.

2 | MATERIALS AND METHODS

2.1 | Site and experimental design

The study site is located in the 100-year-old naturally regenerated Pfynwald forest (46°18 N, 7°36′ E, 615 m a.s.l.), the largest *P. sylvestris L.* dominated forest in Switzerland, located in the dry inner-Alpine valley of the river Rhone, close to the dry edge of the species' natural distribution.

The forest under study is fairly homogeneous, with a mean canopy height of 10.8 m, a stand density of 730 stems ha^{-1} and a basal area of 27.3 m^2 ha^{-1} (Dobbertin et al., 2010). The soil is a calcaric Regosol (FAO classification), characterized by very low water retention and high vertical drainage (Brunner et al., 2009). Climatic conditions are characterized by a mean annual temperature of 10.1°C and a yearly precipitation sum of approximately 600 mm $year^{-1}$.

The experimental site (1.2 ha; ~800 trees) is divided into eight plots of 25 × 40 m^2 each, separated by a 5 m buffer zone. Since 2003, four of these plots have been irrigated with ~600 mm $year^{-1}$ applied at night between April and October, with sprinklers at 1 m height using water from a nearby channel running parallel to the experimental plot and fed by the Rhone river (Figure 1b). Nutrient input through irrigation was proven to be minor (Thimonier et al., 2010). At the end of 2013, irrigation was stopped in a fraction (subplot) of the formerly irrigated plots, corresponding to approximately one-third of the area of the irrigated plots. The irrigation-stop subplots are located upslope from the irrigated plots (i.e., the terrain has a 6° slope, with lower ground on the side of the channel). This resulted in three treatments: control (non-irrigated), corresponding to the trees exposed to naturally dry conditions; irrigated, corresponding to trees released from soil drought for the entire duration of the experiment; and irrigation-stop, corresponding to trees that, after having acclimated to well-watered conditions for 11 years, were once again exposed to drought for 5 years. In 2015, nine scaffolds (three per treatment) were installed in the forest to enable access to tree crowns for sampling and in situ measurements (Figure 2a).

Measurement campaigns were performed three times a year for two consecutive years (2019 and 2020) during spring, summer and autumn. Campaigns included same-day drone flights for the acquisition of multispectral imagery to derive canopy level PRI, needle-level gas exchange and fluorescence measurements to obtain physiological parameters and needle sampling for laboratory pigment quantification. Needle-level measurements and sampling were performed only in the (sub)plot areas equipped with scaffolds, that is, three per treatment (Figure 2a). The selection of sunny measurement days, in combination with the experimental design including irrigated and non-irrigated treatments, made it possible to distinguish between the effect of light only versus the effect of light plus water stress. This is because PRI reflects light stress in general, but in particular, an imbalance between light energy absorbed and light energy that can be used for photosynthesis, the latter depending on water availability.

2.2 | Environmental measurements

Meteorological data were recorded from the top of a 13-m-high scaffold, positioned 1–2 m above the tree canopy; these data are thus available only at the site level and not for individual (sub)plots or treatments (Figure 1a). Air temperature (Sensirion, Stäafa, Switzerland), relative humidity (Sensirion) and precipitation (tipping bucket rain gauge 52,203, Young, MI) were continuously recorded at 10 min intervals. Data from meteorological stations of MeteoSwiss (www.meteoswiss.admin.ch) located ~25 km from Sion were used for gap-filling and instrument error corrections.

Since 2014, 18 soil profiles have been equipped with volumetric soil water probes (10 HS, Decagon Devices, Pullman, WA) and soil water potential (SWP) probes (MPS-2, Decagon Devices) at 10 and 80 cm soil depth. Three (sub)plots for each treatment were equipped with two sensors each. Measurements are continuously recorded at 15 min intervals, and data calibration is performed in the post-processing to normalize for the temperature sensitivity of the MPS-2 sensors (Walthert & Schleppi, 2018).

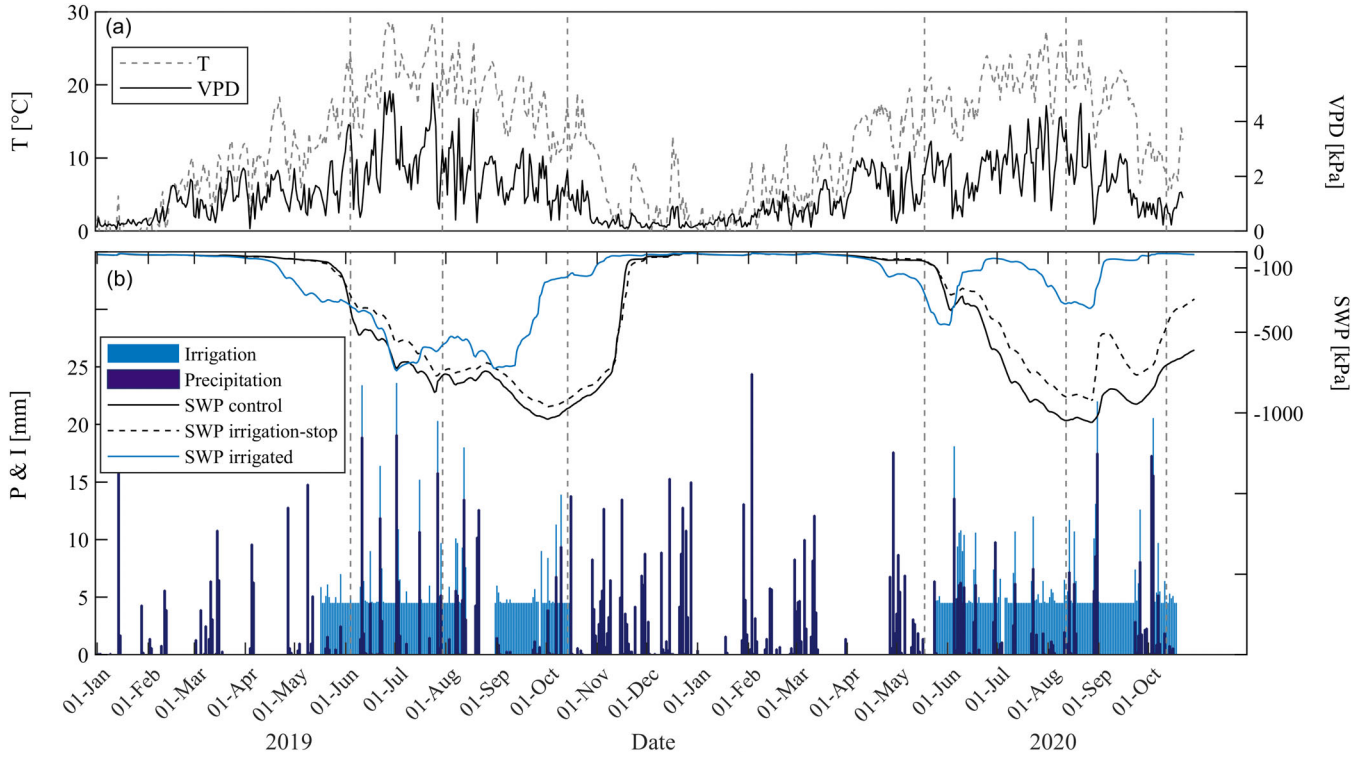

FIGURE 1 Environmental parameters at the Pfynwald forest experimental site over the two measurement years: (a) daily mean temperature (T) and daily maximum VPD, (b) daily irrigation superimposed on natural precipitation and daily mean soil water potential (SWP) measured at 80 cm depth for control, irrigation-stop and irrigated treatments. Dashed vertical lines identify dates of the drone and field campaigns [Colour figure can be viewed at wileyonlinelibrary.com]

2.3 | Drone flights and photochemical reflectance index

Narrow-band multispectral imagery was collected using a modified Micasense camera (Micasense, Seattle, WA) mounted on a DJI Matrice 100 quadrocopter (DJI Technology Co., Ltd., Shenzhen, China). The camera comprises five separate imaging sensors that operate nearly simultaneously in five narrow custom bands in the visible and near-infrared part of the electromagnetic spectrum, chosen to target specific photosynthetic pigment absorption features (Table S1). A customized angled attachment compensates for the tilt derived from a flight forward movement, so that the camera keeps a close-to-nadir orientation to the surface during image acquisition. Drone flights were conducted under sunny, clear sky conditions within 2 hr of local solar noon to minimize shadows and large variations in acquisition geometry and to improve the data signal-to-noise ratio. As an exception, morning and afternoon flights conducted around 10 and 15 CET, respectively, were included in the diurnal analysis. Drone image processing, including georeferencing, reflectance calibration and orthomosaic generation, was performed using the commercial Agisoft PhotoScan package (Agisoft LLC, St. Petersburg, Russia, 191,144). Georeferencing was supported by 11 ground control points (GCPs) whose coordinates were measured in the field using a differential Global Navigation Satellite System (dGNSS). Reflectance calibration was performed using images of a gray reference panel reflecting 60% of the incident light (Micasense, Seattle, WA), taken from the ground before and after each flight. Orthomosaics were generated with the blending mode set to disabled; this option uses the original pixel value taken from the photo with the camera view along the normal to the reconstructed surface in that point. The difference between the digital surface model (DSM) and the digital terrain model (DTM), both generated from the dense point cloud in Agisoft PhotoScan, resulted in the canopy height model (CHM). In ArcGIS (ArcGIS Desktop, Release 10.5, Esri, Redlands, CA, 2011), the CHM was reclassified to a binary layer separating the overstory tree crowns from the background by setting the local minima of the bimodal distribution of all scene's pixels as the threshold. For all dates, the local minimum was identified to be around 5 m above the ground, which, given the stand mean canopy height of 10.8 m, was considered a realistic threshold. The resulting background masks were applied to the orthomosaics to exclude pixels belonging to ground, understory vegetation and young tree individuals from further analysis.

In the next step, a shade mask was generated from the near-infrared (NIR) band at 900 nm clipped to the study area. A reclassification to a binary layer separating shaded from sunlit pixels was performed by setting the local minima of the bimodal distribution of all overstory scenes' pixels as a threshold (Otsu, Pla, Duane, Cardil, & Brotons, 2019). The local minima used as threshold varied slightly from date to date, as the fraction of shaded crown pixels changes depending on the sun angle over the day and season. The resulting shade masks were applied to the orthomosaics to exclude from further analysis pixels belonging to shaded parts or openings

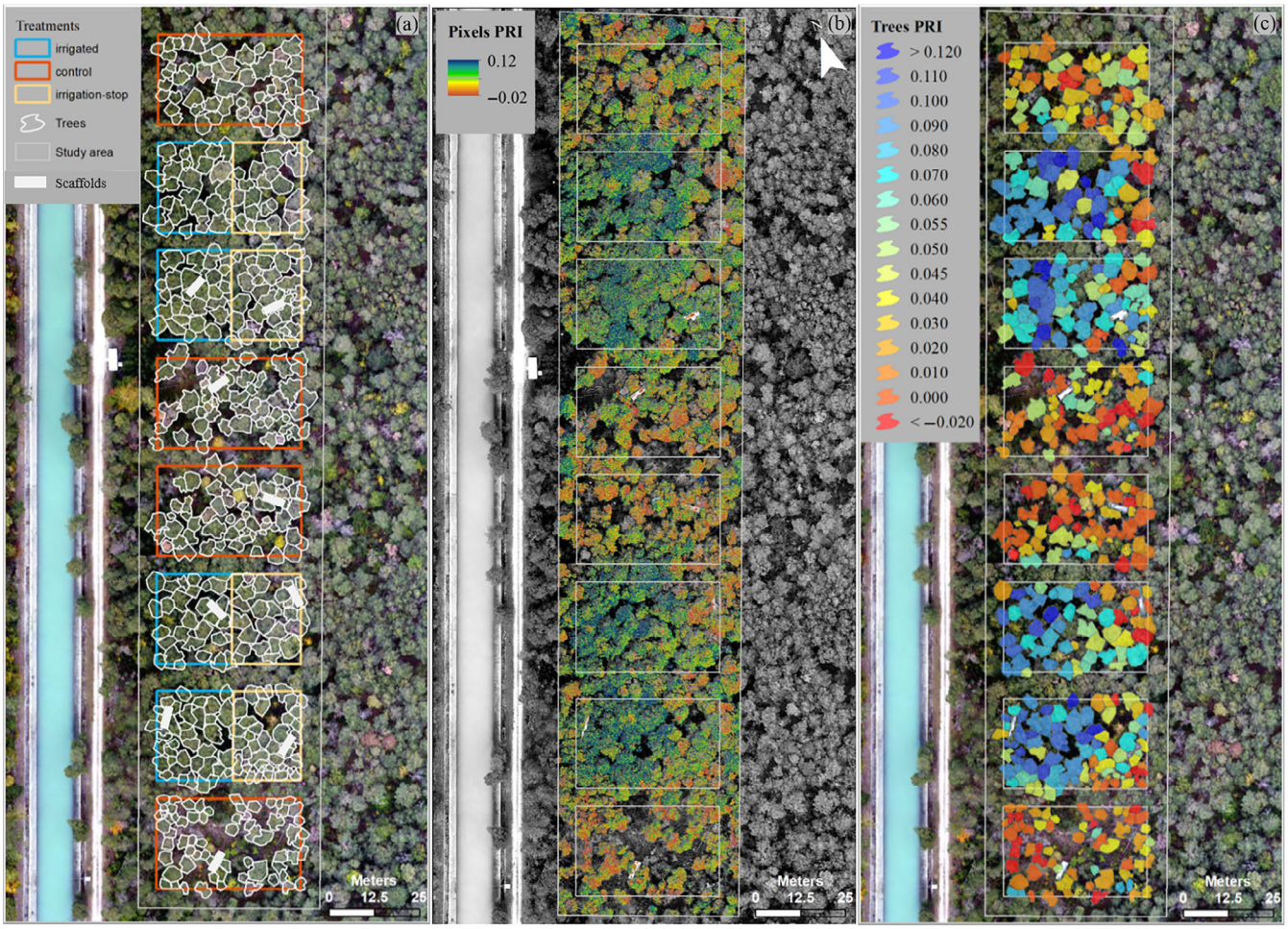

FIGURE 2 Remotely sensed photochemical reflectance index (PRI) from drone-based multispectral imagery acquired on 12 August 2020 over a *Pinus sylvestris* forest at the long-term precipitation manipulation (irrigation) experiment in Pfynwald (Canton Valais), Switzerland. The experimental plot design distinguishing three treatments (control, irrigation-stop, irrigated) is shown on the left (a), including tree crown polygons and scaffold positions. Pixel-level and tree-level PRI maps are shown in the centre (b) and on the right (c), respectively [Colour figure can be viewed at wileyonlinelibrary.com]

within the crowns, which might also vary regarding crown transparency.

The photochemical reflectance index (PRI) was computed as the normalized difference of reflectance at 531 nm, which is reduced by the de-epoxidation of xanthophyll pigments, and reflectance at 570 nm, which is largely insensitive to changes in the xanthophyll cycle (Gamon et al., 1992):

$$\mathrm{PRI} = (R_{531\mathrm{nm}} - R_{570\mathrm{nm}})/(R_{531\mathrm{nm}} + R_{570\mathrm{nm}}), \quad (1)$$

where R stands for reflectance at the specific wavelength.

Tree crown delineation was performed via visual interpretation of a high-resolution true colour orthomosaic obtained via a drone flight in October 2019, when phenological differences between *P. sylvestris* and the few broadleaf tree species present in the plots (e.g., *Quercus pubescens* WILLD.) are most evident (Figure 2a). Broadleaf trees and mistletoe-infested parts of the *P. sylvestris* crowns, were visually identified in the imagery and masked out for further analysis. Tree positions were further compared with positions obtained through tachymeter measurements. The tree crowns polygon vector layer was then used with the pixel PRI raster layer (Figure 2b) in the Zonal Statistics tool of ArcGIS to compute PRI crown mean values (Figure 2c). This procedure allows one representative PRI value per tree to be obtained, irrespective of differences in crown size and despite intra-crown variation. (Sub)plot-level PRI estimates were obtained by averaging PRI values of trees within a (sub)plot, while treatment-level PRI estimates were calculated by averaging the PRI values of all (sub)plots in each treatment.

2.4 | Gas exchange and fluorescence measurements

The percentage of absorbed light that is used in photochemistry or dissipated as heat can be estimated by chlorophyll fluorescence measurements at the leaf scale, making it possible to estimate physiological parameters linked with trees' photosynthesis and photoprotective processes on the days of drone surveys.

Leaf gas exchange and chlorophyll fluorescence were measured simultaneously from the top of the scaffolds on attached branches, using portable infrared gas analysers with a multiphase flash fluorometer (LI-6800; LI-COR Inc., Lincoln, NE) and a 6-cm^2 leaf cuvette. In each of the six campaigns, measurements were performed between 10:00 and 17:30 CET over 2.5 days centred around the drone flights. Environmental conditions stayed relatively stable throughout each campaign (Figure S1). On each scaffold, a minimum of three trees (one branch per tree) were measured, resulting in nine trees per treatment, except for the first spring campaign, during which we measured three branches per tree but reduced the number of trees measured per treatment to five. This early sampling design was changed for the later campaigns because inter-tree variation was greater than intra-tree variability. In both years, we conducted measurements on the previous year's needles because of the potential for differences in the timing of phenology of the current year's needles to confound any treatment effects. The measurement protocol included a 30-min dark adaptation of the attached twigs wrapped in aluminium foil. The previous year's needles of sun-exposed, top-of-crown twigs were then placed inside the cuvette and left to acclimate in the dark for an additional 10 min. Inside the cuvette, vapour pressure deficit (VPD) was set to 1.5 kPa, CO_2 to ambient 400 ppm and temperature to 20°C with adjustments of a few degrees to approximate changes in the ambient environment throughout the season.

We used pulse-amplitude modulated (PAM) fluorescence with the rectangular flash setup to obtain dark- and light-adapted fluorescence parameters. A saturating pulse, with an intensity of 10,000 μmol m^{-2} s^{-1} for 700 ms, was applied to obtain dark-adapted parameters like minimum fluorescence (F_o) and maximum fluorescence (F_m), from which maximum quantum yield (F_v/F_m) was calculated according to Genty, Briantais, and Baker (1989) as:

$$F_v/F_m = (F_m - F_o)/F_m. \quad (2)$$

After maximum quantum yield determination, light in the cuvette was first increased to 400 and then to 1,500 μmol m^2 s^{-1}, and the saturating pulse was applied to determine light-adapted fluorescence parameters after stabilization of leaf gas exchange for approx. 10 min. Specifically, the fraction of light that is thermally dissipated via dynamic non-photochemical quenching (NPQ) was calculated according to Demmig-Adams (1998) as:

$$NPQ = F_s/F_m' - F_s/F_m, \quad (3)$$

where F_s is steady-state fluorescence in a light-adapted sample recorded just before each saturating pulse, and F_m' is the maximum fluorescence of light-adapted needles.

Gas exchange parameters, like photosynthesis (A) and stomatal conductance (g_s), were measured at the end of the cycle under 1,500 μmol m^2 s^{-1} saturating light conditions. After each measurement, the part of the needles enclosed in the cuvette was harvested, and the projected leaf area was determined using a flatbed scanner and the software Pixstat v1.3.0.0 (Schleppi, 2018). The projected leaf area of the measured needles was used to correct the recorded gas exchange values.

2.5 | Photosynthetic pigments

Needle samples were collected during a 2 hr period centered around the time of a midday drone flight. Needles were taken from the same three trees and the same sun-exposed south-facing branches on which gas exchange and fluorescence measurements were performed. Needle samples were flash frozen in the field in dry ice and stored at −80°C in the lab. Pigment analysis was performed according to Junker and Ensminger (2016). Frozen needles were ground to a fine powder in liquid nitrogen, and pigments were then extracted in the dark in 98% methanol buffered with 2% of 0.5 M ammonium acetate for 2 hr. Extracts were then filtered through a 0.45 μm polytetrafluoroethylene filter, prior to the separation of the pigments by high-performance liquid chromatography (HPLC) using an Agilent Infinity Quaternary LC system (Agilent Technologies, Deutschland GmbH & Co. KG, Waldbronn, Germany) and a C30-column (5 μm, 250 × 4.6 mm^2, YMC Inc., Wilmington, NC). Total carotenoid content was calculated as the sum of the amount of violaxanthin (V), antheraxanthin (A), zeaxanthin (Z), neoxanthin, lutein, α-carotene and β-carotene. Total carotenoids were normalized to the sum of chlorophyll a plus chlorophyll b and expressed as Car/Chl in mmol mol^{-1}. Total xanthophylls were calculated as V + A + Z (VAZ), and the de-epoxidation status (DEPS) of the xanthophyll cycle pigments was calculated according to Thayer and Björkman (1990) as:

$$DEPS = (0.5A + Z)/(V + A + Z). \quad (4)$$

2.6 | Statistical analysis

2.6.1 | Correlation analysis between remotely sensed PRI and leaf-level physiology

We investigated the (up-)scalability of physiological processes, such as pigments adjustments and photosynthesis, from the leaf to the tree level by means of our remotely sensed proxy PRI. The strength and direction of the linear relationships between leaf-level measurements and tree-level PRI were investigated using correlation analysis. Leaf-level measurements were acquired on the same day as drone imagery. As an exception, in spring 2020, a temporal offset of a few weeks occurred, due to technical problems with the equipment, which led to the exclusion of this time point from the correlation analysis, despite comparable environmental conditions.

2.6.2 | Significance analysis of treatment differences in tree response

We tested the significance of treatment differences (control, irrigated, irrigation-stop) in the PRI tree response, as well as in gas exchange

and pigments parameters using a two-sample *t*-test. Treatment differences were tested for each date separately to investigate seasonal dependencies, using linear mixed-effects models in Matlab (version 9.5.0 R2018b). Treatment was considered a fixed effect and introduced as a categorical variable, while (sub)plot was introduced as a random effect influencing the model intercept to control for repeated measurements and for potential (sub)plot effects.

2.6.3 | Analysis of acclimation and environmental drivers on tree PRI

The effect of potential drivers on PRI tree responses, particularly the effect of concurrent environmental conditions versus the effect of long-term acclimation resulting from treatment, was tested over seasonal timescales for the 2 years. A linear mixed-effects model fitted with maximum likelihood (ML) was selected following the top-down approach suggested by Zuur, Ieno, Walker, Saveliev, and Smith (2009), as well as our understanding of the biological problem. The starting point was a model where the fixed component contained all explanatory variables, namely treatment, mean daily SWP measured at 80 cm depth and maximum daily VPD, and all their interactions. Environmental parameters were taken as the average value over the 5 days preceding a drone flight. Date and (sub)plot number were chosen as random effects influencing the model intercept in a crossed design, according to our experimental setup (Table S5). Date was introduced to control for potential phenology effects. The fixed part of the mixed-effects model was selected by sequentially removing non-significant terms. All possible reduced models were compared based on the Akaike information criterion (AIC) and Bayesian information criterion (BIC) values to obtain the minimum adequate model. When several models showed ΔAIC ≤ 2, the simplest model was chosen. If an interaction effect was significant, the corresponding individual-fixed effects were included in the model regardless of their significance or the model AIC value (see Tables S2 and S3 for details on model selection). The optimal model was refitted using the restricted maximum likelihood (REML) method to obtain estimates and significances of effects (Table 1). REML was chosen because it is known to be more robust in accommodating unbalanced designs characterized by an unequal number of observations, as is common in ecological studies (Spilke, Piepho, & Hu, 2005). In our study, the control, irrigation-stop and irrigated treatments included 197, 111 and 105 trees, respectively, corresponding to the tree crowns that were identified based on drone RGB imagery and ground tree coordinates. Homoscedasticity and normality of residuals were verified visually.

The effect of potential drivers on PRI tree responses was also tested over diurnal timescales by including all summer dates for which drone flights were performed at different times of the day (i.e., ~10:00, 12:30 and 15:00 CET). For this analysis, we started by comparing two models, fitted with ML, with treatment and time of day as fixed effects, with and without the interaction term, to verify whether diurnal cycles of environmental parameters affect the sensitivity of the PRI – treatment relationship. In a second step, we replaced time of day with environmental parameters (VPD, photosynthetically active radiation [PAR] and SWP at 10 cm depth), averaged over the hour centered around a drone flight, to understand which parameters best explain PRI diurnal variability (Table S5). We used SWP from shallower soil here as we were interested in

TABLE 1 Seasonal effects of a precipitation manipulation (irrigation) treatment and environmental parameters on the drone-based remotely sensed photochemical reflectance index (PRI) at the Pfynwald *Pinus sylvestris* experimental forest site for all dates ($N = 54$) based on a linear mixed-effects model

Model: PRI ~ 1 + treatment × SWP_{5d} + (1 | plot) + (1 | date)							
Fixed effects	**Estimates**	***SE***	***t*-value**	**DF**	***p*-value**	**Random**	***SD***
Intercept	0.062	0.008	7.565	50	<.001	Plot	0.010
						Date	0.007
Treatment							
IS	−0.004	0.010	−0.406		.687		
I	−0.003	0.010	−0.294		.769		
SWP_{5d}	3.681e-05	6.853e-06	5.372	50	<.001		
Treatment: SWP_{5d}							
IS:SWP_{5d}	−2.162e-05	8.927e-06	−2.423	50	<.05		
I:SWP_{5d}	−5.902e-05	1.251e-05	−4.716	50	<.001		
Residual error							0.009

Note: Soil water potential (SWP) was measured at 80 cm depth and averaged over the 5 days preceding a drone acquisition. Treatments include control (C), corresponding to trees exposed to the naturally dry conditions and used as a reference in the model; irrigation-stop (IS), corresponding to trees exposed to drought again after acclimation to irrigation; and irrigation (I), corresponding to trees released from soil drought for the entire duration of the experiment. (1 | effect), random effect for the model intercept; effect1 × effect2, fixed effect1, fixed effect2 and their interaction effect1:effect2; effect1:effect2, interaction effect; estimates, model coefficients for each of the fixed effects and their interactions; *SE*, standard error of the estimates; *SD*, standard deviation of the random effects.
Abbreviations: PRI, photochemical reflectance index; SWP, soil water potential.

short-term responses more related to the conditions in shallower and more dynamic soil horizons. The optimal model was refitted using the REML method to obtain estimates and significances of effects (Table 2).

3 | RESULTS

3.1 | Environmental parameters

At the Pfynwald study site, VPD ranged from 0 to 4 kPa (Figure 1a) and SWP at 80 cm depth varied between 0 and −1,000 kPa (Figure 1b) over the course of the year. In winter, when irrigation was switched off, SWP was comparably high over all treatments. In spring before the start of irrigation, SWP in the irrigated plots dropped below that in non-irrigated (sub)plots (i.e., control and irrigation-stop treatment) because irrigated trees with their larger crowns have higher evapotranspiration rates. In 2019, this trend persisted through the summer with SWP values in irrigated plots nearly matching those of non-irrigated (sub)plots. Treatment differences were further reduced in this period, due to malfunctioning of the irrigation system over a few weeks in August 2019 (Figure 1b). On the other hand, summer 2020 was characterized by the expected differences in soil water availability between treatments, with higher soil water availability for trees in irrigated plots, while SWP dropped to the critical level of −1,000 kPa in non-irrigated plots and subplots. Autumns were characterized by increases in SWP in irrigated plots, while in the two non-irrigated treatments water availability remained low for both years.

3.2 | Treatment differences in the remotely sensed PRI tree response

In spring, drone-based PRI tree responses showed the smallest differences among treatments, with relatively high PRI values indicating high photochemical efficiency of trees not experiencing drought stress. While, treatment still explained 50% of the variance in spring PRI in 2019 (Table S2), in 2020, we found no significant differences among spring PRI values (Figures 3a,d and 4a,d).

In summer, we observed the largest PRI tree response differences among treatments, with control (C) trees showing significantly lower PRI values than irrigation-stop (IS) trees (for which irrigation was stopped 5 years ago), which in turn showed significantly lower PRI values than irrigated (I) trees (Figure 4b,e). In 2019, this was caused mainly by drought stress release in irrigated trees (i.e., higher PRI) compared with spring and a stress increase in control trees (i.e., lower PRI), while irrigation-stop trees maintained similar PRI values in summer as in spring. In 2020, on the other hand, PRI differences among treatments originated mainly from a stress increase (i.e., lower PRI) in non-irrigated trees in summer compared with at the beginning of the growing season (Figures 3b,e and 4b,e). Summer 2020 saw the largest significant ($p < .001$) PRI differences ($PRI_C = 0.01 \pm 0.01$; $PRI_{IS} = 0.04 \pm 0.01$; $PRI_I = 0.08 \pm 0.004$) among treatments compared with any other date (Figures 3e and 4e, Table S2).

In autumn 2019, PRI differences among treatments were significant ($p < .05$; Figures 3c and 4c), with treatment explaining 70% of the observed variance (Table S2), while in autumn 2020, no significant difference was detected in PRI values (Figures 3f and 4f).

3.3 | Relationships between remotely sensed PRI and leaf-level physiology

3.3.1 | Pigments seasonality

Non-irrigated trees (i.e., control and irrigation-stop) showed overall larger carotenoid and xanthophyll cycle pigments pool sizes in relation to chlorophyll pools, that is, Car/Chl in summer 2020 (Figure S1k) and VAZ/Chl in spring and summer 2020 (Figure S1p,q), indicating an increased capacity for energy dissipation. Similarly, the de-epoxidation

TABLE 2 Diurnal effects of precipitation manipulation (irrigation) treatment and environmental parameters on drone-based remotely sensed photochemical reflectance index (PRI) at the Pfynwald *Pinus sylvestris* experimental forest site for three summer days ($N = 68$) based on a linear mixed-effects model

Model: PRI ~ 1 + treatment + VPD + (1 | plot)							
Fixed effects	**Estimates**	***SE***	***t*-value**	**DF**	***p*-value**	**Random**	***SD***
Intercept	0.070	0.011	6.419	68	<.001	Plot	4.883e-18
Treatment							
IS	0.026	0.006	4.180	68	<.001		
I	0.053	0.006	8.399	68	<.001		
VPD	−0.012	0.004	−3.065	68	<.01		
Residual error							0.022

Note: Vapour pressure deficit (VPD) is averaged for 1 hr centered around a drone acquisition. Treatments include control (C), corresponding to trees exposed to the naturally dry conditions and used as reference in the model; irrigation-stop (IS), corresponding to trees exposed to drought after acclimation to irrigation; and irrigation (I), corresponding to trees released from soil drought for the entire duration of the experiment. (1 | effect), random effect for the model intercept; effect1 × effect2, fixed effect1, fixed effect2 and their interaction effect1:effect2; effect1:effect2, interaction effect; estimates, model coefficients for each of the fixed effects and their interactions; *SE*, standard error of the estimates; *SD*, standard deviation of the random effects.

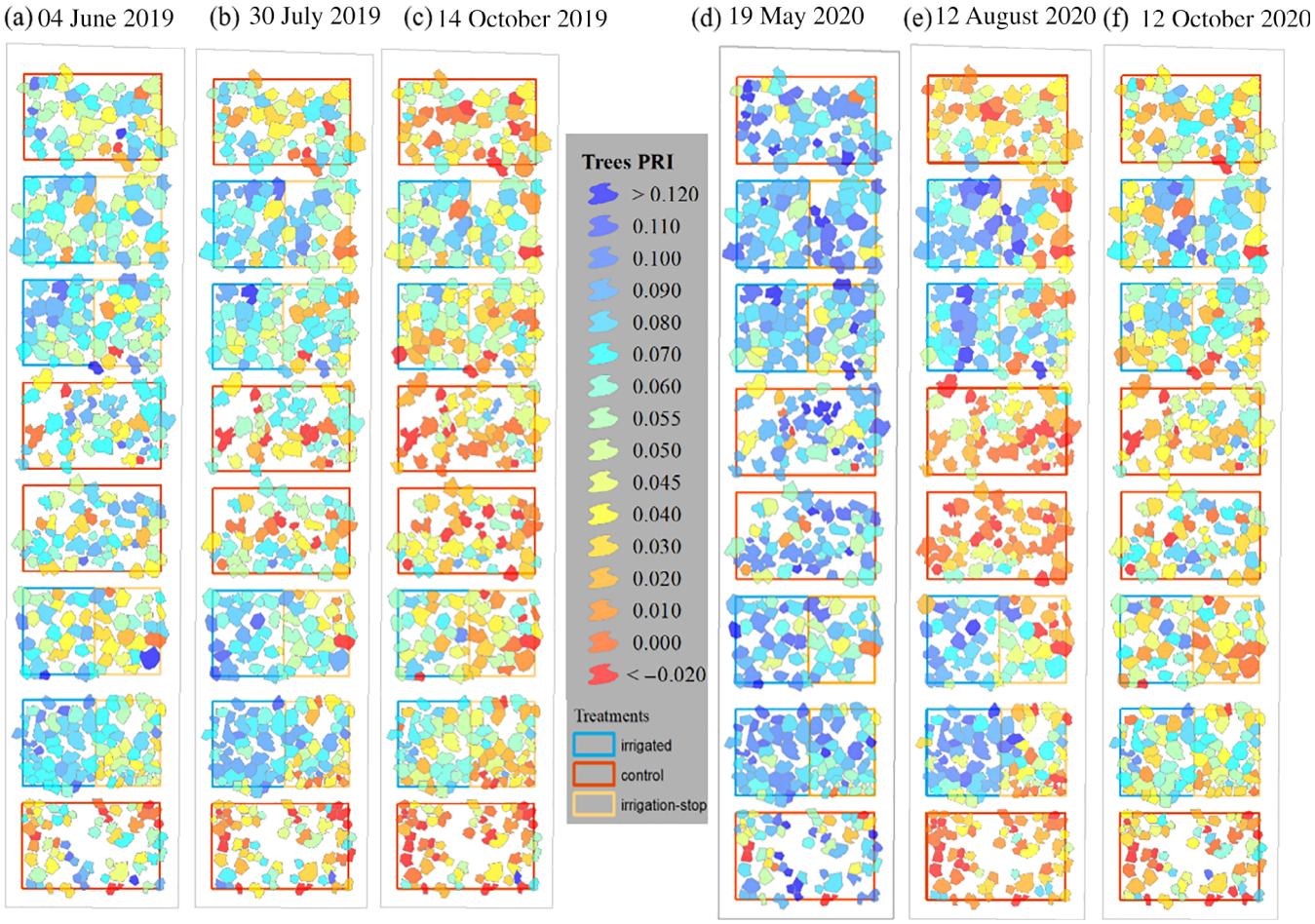

FIGURE 3 Spatial distribution of the tree-level remotely sensed photochemical reflectance index (PRI) at the Pfynwald *Pinus sylvestris* forest experimental site, over two growing seasons. Precipitation manipulation (irrigation) treatments include control, corresponding to trees exposed to the naturally dry conditions; irrigation-stop, corresponding to trees that were exposed to drought again after acclimation to irrigation; and irrigation, corresponding to trees released from soil drought for the entire duration of the experiment. PRI was obtained from drone-based multispectral imagery acquired under clear-sky conditions near midday. PRI tree-level values represent within-crown averages [Colour figure can be viewed at wileyonlinelibrary.com]

status of the xanthophyll cycle pigments (DEPS) was significantly higher for non-irrigated trees than for irrigated in spring 2019 and summer 2020, indicating an enhanced efficiency of energy dissipation in non-irrigated trees (Figure S1a,e).

Significant correlations were found between all three leaf-level pigment parameters and drone-based tree-level PRI when all dates and treatments were pooled together (Figure 5a,e,i). The best correlation was with DEPS ($r^2 = 0.37$, $p < .001$), followed by Car/Chl ($r^2 = 0.24$, $p < .001$), and VAZ/Chl ($r^2 = 0.14$, $p < .05$). In summer, we found the highest correlations between drone-based PRI and pigment parameters (Figure 5c,g,k), with the strongest relationship being the one between PRI and DEPS ($r^2 = 0.56$, $p < .001$). In autumn, the significant correlation of PRI with DEPS and VAZ persisted, while there was no correlation between PRI and Car/Chl (Figure 5d,h,l). Analysis for spring 2019 revealed no significant correlations (Figure 5b,f,j), while spring 2020 data were omitted from this analysis, as drone flights and needle collection were offset by a few weeks due to technical problems with the equipment.

3.3.2 | Gas exchange and fluorescence

Gas exchange and fluorescence measurements confirmed what was observed with all other measurements, namely that the greatest differences between treatments occurred in summer 2020. Reference trees mean values of A, g_s, F_v/F_m and Θ_{PSII} were significantly ($p < .05$) higher for irrigated than for non-irrigated (control and irrigation-stop) trees, while NPQ was lower (Figure S3). Among all parameters, irrigated trees showed higher values than non-irrigated trees most consistently across seasons and years for g_s (Figure S3g–l). NPQ treatment differences were also rather persistent across all seasons, with a few dates (autumn 2019 and summer 2020) for which significant differences appeared especially for irrigation-stop versus irrigated trees (Figure S3y–dd).

Over summer, we observed significant correlations between all leaf-level physiological parameters and drone-based tree-level PRI values averaged at the (sub)plot level, while only weak correlations were present when considering all dates (data not shown). Comparing

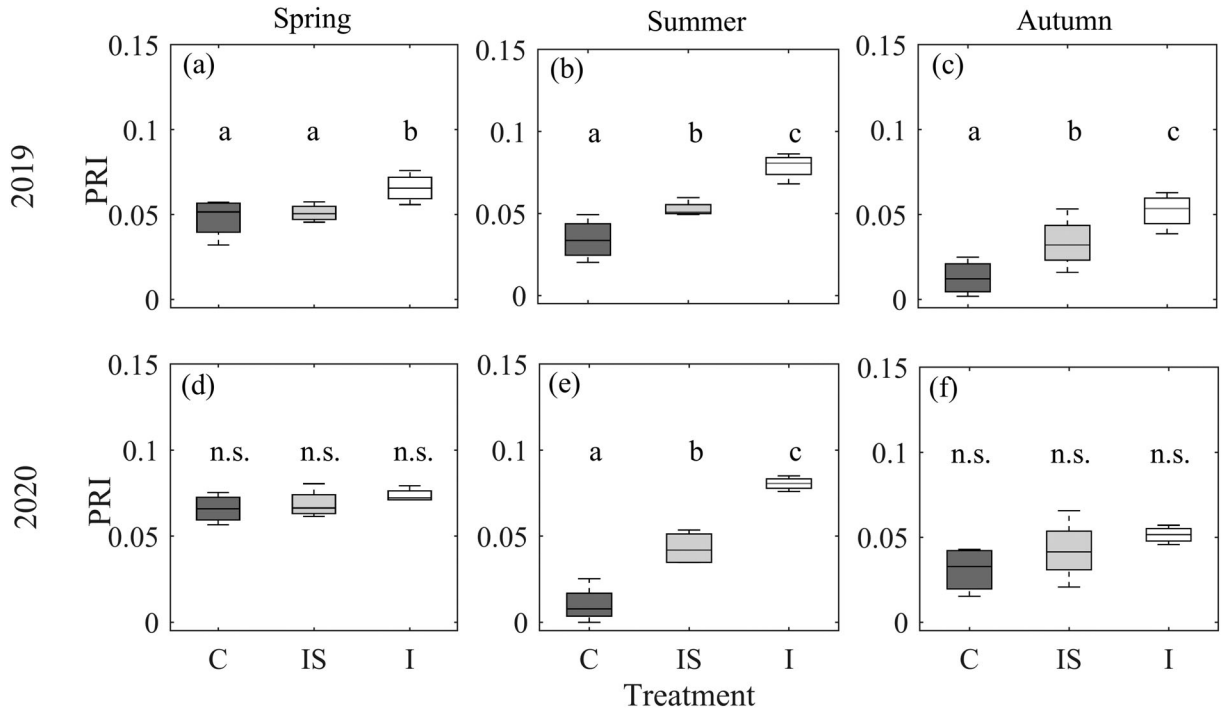

FIGURE 4 Remotely sensed photochemical reflectance index (PRI) differences among precipitation manipulation (irrigation) treatments at the Pfynwald *Pinus sylvestris* experimental forest site. Treatments include control (C), corresponding to trees exposed to the naturally dry conditions; irrigation-stop (IS), corresponding to trees that were exposed to drought again after acclimation to irrigation; and irrigation (I), corresponding to trees released from soil drought for the entire duration of the experiment. PRI was obtained from drone-based multispectral imagery acquired over two growing seasons, under clear-sky conditions near midday, on (a) 04 June 2019, (b) 30 July 2019, (c) 14 October 2019, (d) 19 May 2020, (e) 12 August 2020 and (f) 12 October 2020. Letters above the boxplots indicate significant differences between treatments ($p < .05$, with n.s. indicating not significant) according to linear mixed-effects models, with treatment as a fixed effect and (sub)plot number as a random effect

the two summers, the strongest correlations occurred in 2020 (Figure 6), when *A* and g_s were close to zero in non-irrigated trees but in the order of 5.7 μmol m^{-2} s^{-1} (*A*) and 0.03 mol m^{-2} s^{-1} (g_s) for irrigated trees, showing good correlations with drone-based tree-level PRI (*A*: $r^2 = 0.77$, $p < .01$; g_s: $r^2 = 0.47$, $p < .05$; Figure 6a,b). Similarly, strong correlations in summer 2020 existed between PRI and F_v/F_m ($r^2 = 0.65$, $p < .01$; Figure 6c), Θ_{PSII} ($r^2 = 0.62$, $p < .05$; Figure 6d) and NPQ ($r^2 = 0.41$, $p = .061$; Figure 6e).

3.4 | Drivers of remotely sensed PRI dynamics

3.4.1 | Seasonal timescale

Over the seasonal timescale, the drone-based PRI tree response followed the seasonal course of soil water availability for non-irrigated trees (Figure 7a,b). Daily mean SWP at 80 cm depth, averaged over the 5 days preceding a drone flight, was the best predictor of mid-day (sub)plot-level PRI ($p < .001$; Table 1). The explanatory power of SWP varied as a function of treatment type, as shown by the significance ($p < .001$, Table S4) of the interaction term. An increase in SWP of one unit corresponded to an increase in PRI of 3.7e-05 for a tree exposed to the naturally dry conditions (i.e., in control plots), while the rate of PRI increase was slightly lower for trees in irrigation-stop subplots, significantly negative ($p < .05$) for irrigated trees (Figure 7c).

As shown from the ANOVA results of the four evaluated statistical models (Table S4), irrigation treatment alone and, among the environmental parameters, daily maximum VPD averaged over the 5 days preceding a drone flight did not explain PRI variability over the year. Treatment was kept in the final model because its interaction effect with SWP was significant (Table S3).

3.4.2 | Diurnal timescale

Over the course of the measured summer days, VPD at the top of the canopy varied between 0 and 4 kPa, with peak values typically reached around 15:00 CET, while incoming radiation on clear-sky days reached its maximum value earlier, around 12:30 CET (Figure 8a,b). In contrast, SWP at 10 cm depth is typically characterized by small variations over the course of a clear, sunny summer day, for example, ΔSWP ~25 kPa.

For all treatments, PRI values obtained for ~10:30, 12:30 and 15:00 CET decreased with the time of day (largest drop from morning to midday), in line with the diurnal course of VPD and PAR (Figure 8a,b).

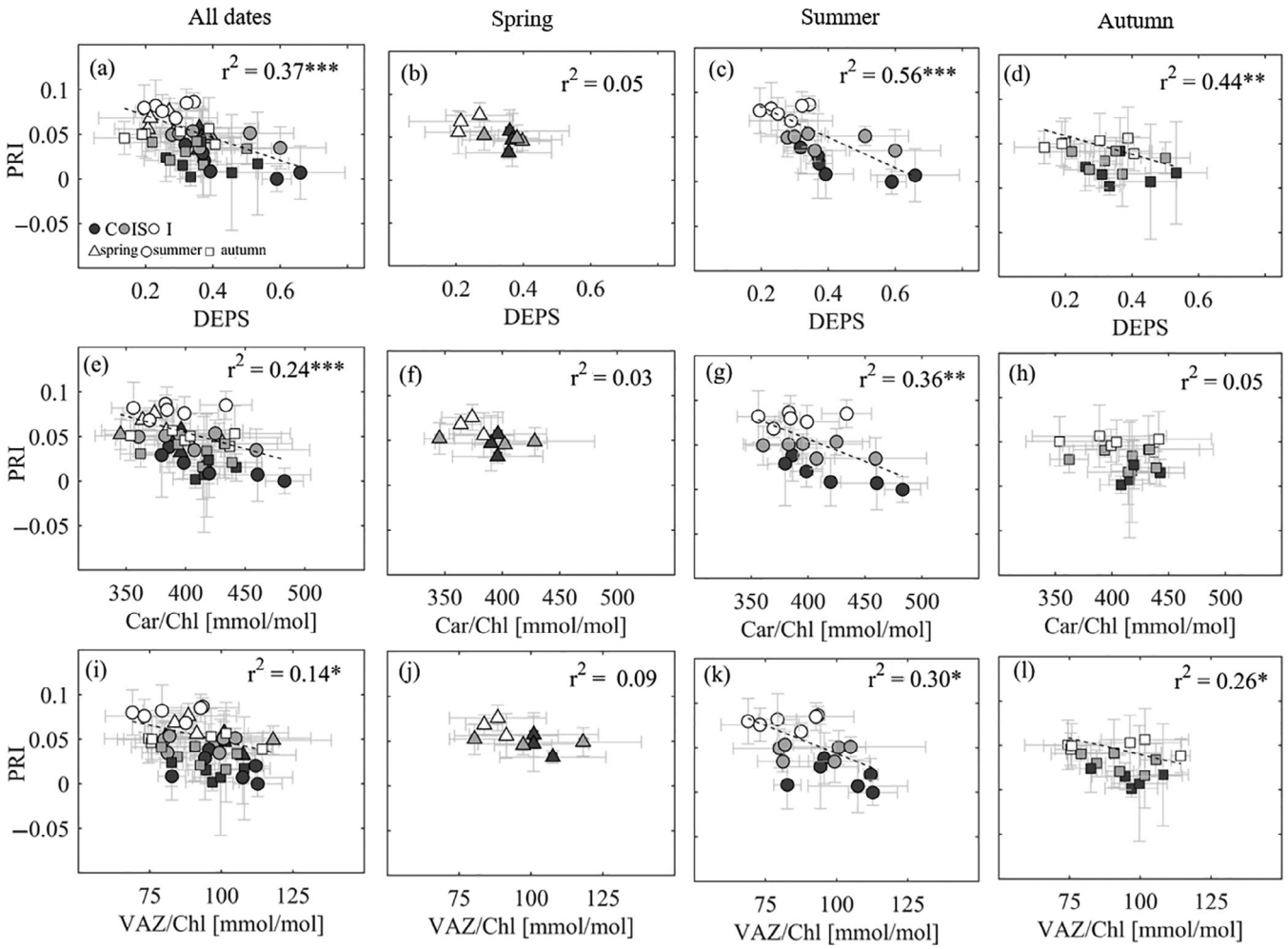

FIGURE 5 Relationship between drone-based tree-level photochemical reflectance index (PRI) and leaf-level (a–d) de-epoxidation state of the xanthophyll cycle (DEPS), (e–h) carotenoid to chlorophyll pool ratio and (i–l) violaxanthin (V) + antheraxanthin (A) + zeaxanthin (Z) to chlorophyll pool ratio, for all dates, for spring (only 2019) and for summer and autumn dates in 2019 and 2020 at the Pfynwald *Pinus sylvestris* experimental forest site. Symbols represent mean values for trees surrounding scaffolds ($n \geq 3$) in each (sub)plot and error bars are *SD*. Precipitation manipulation (irrigation) treatments are represented with different shades of gray: dark for control (C), light for irrigation-stop (IS) and white for irrigated (I). Seasons are represented with different symbols. r^2 values and significance levels are indicated for the linear correlations (dashed regression lines are given for significant relationships; $^*p < .05$, $^{**}p < .01$, $^{***}p < .001$)

The ANOVA indicated that treatment and time both explained (sub)plot-level PRI over the day. Among the environmental parameters varying in time, VPD was found to best explain the concomitant differences in (sub)plot-level PRI, while PAR and SWP at 10 cm depth were not significant and were excluded from the final model (Tables 2 and S5). The environmental parameters were measured at different spatial scales (i.e., site vs. (sub)plot) and spanned different value ranges, which might have influenced their predictive power in the model. No significant interaction was found between treatment and time ($p = .970$; Table S5), indicating that the sensitivity of PRI to environmental parameters over the day does not vary across treatments. The linear regression analysis between PRI and VPD demonstrated that the intercept, but not the slope, of this relationship was dependent on treatment (Figure 8c).

4 | DISCUSSION

4.1 | PRI as a physiological proxy for tracking drought stress and recovery

Remote sensing vegetation indices related to structure and greenness, such as the normalized difference vegetation index (NDVI), are not sensitive to rapid adjustments in plant photosynthetic status in response to environmental stressors and do not allow real-time physiological monitoring of plants (Zarco-Tejada, Morales, Testi, & Villalobos, 2013). Carotenoid-sensitive spectral indices, such as PRI and the chlorophyll/carotenoid index (CCI), are instead directly linked to the (de)epoxidation status of xanthophyll cycle pigments and the process of safe excess energy dissipation under drought (D'Odorico, Besik, Wong, Isabel, & Ensminger, 2020; Gamon et al., 1990; Peñuelas, Filella, & Gamon, 1995;

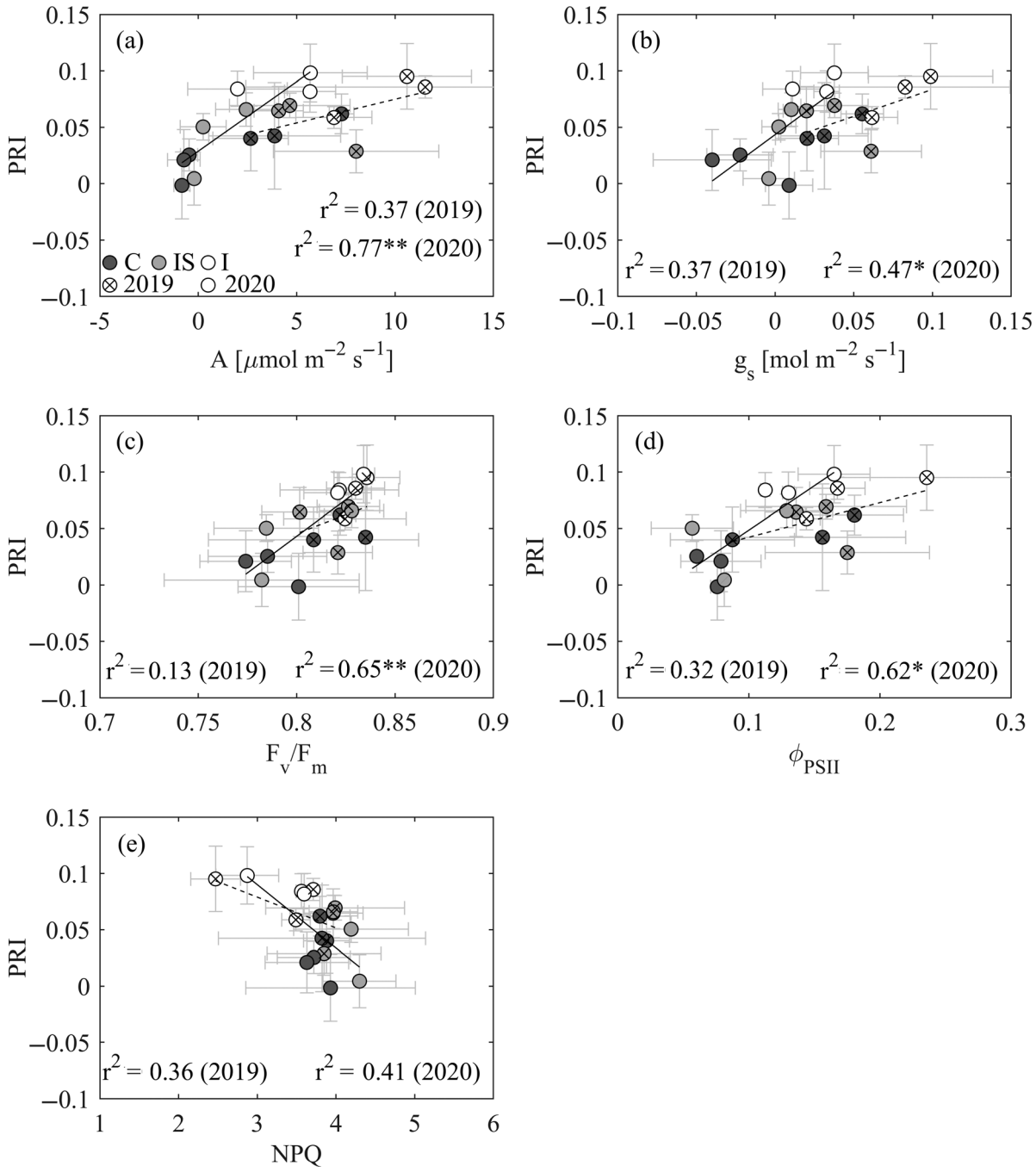

FIGURE 6 Relationship between drone-based tree-level photochemical reflectance index (PRI) and leaf-level (a) photosynthesis (*A*) at 1,500 μmol m^{-2} s^{-1}, (b) stomatal conductance (g_s), (c) maximum quantum yield of PSII (F_v/F_m), (d) quantum yield of PSII (Θ_{PSII}) and (e) non-photochemical quenching (NPQ), over the summer season of 2 years (2019, 2020) at the Pfynwald *Pinus sylvestris* experimental forest site. Circles are mean values for trees surrounding scaffolds ($n \geq 3$) in each (sub)plot and error bars are *SD*. Precipitation manipulation (irrigation) treatments are represented with different shades of gray: dark for control (C), light for irrigation-stop (IS) and white for irrigated (I). Years are represented with different symbols (cross = 2019, solid = 2020) and line types (dashed = 2019, solid = 2020). r^2 values and significance levels are indicated for the linear correlations (*p < .05, **p < .01, ***p < .001)

Wong et al., 2020). Among the carotenoid-sensitive indices, PRI was most successful in capturing changes in photochemical efficiency over short timescales and was thus selected over CCI for this study. Its potential as a proxy for monitoring drought stress has been amply investigated for Mediterranean vegetation, where summer drought represents the primary environmental constraint (Goerner, Reichstein, & Rambal, 2009; Hernández-Clemente, Navarro-Cerrillo, Suárez, Morales, & Zarco-Tejada, 2011; Marino et al., 2014; Peguero-Pina, Morales, Flexas, Gil-Pelegrín, & Moya, 2008; Peñuelas, Munné-Bosch, Llusià, & Filella, 2004; Stylinski, Gamon, & Oechel, 2002; Yang et al., 2020; Zarco-Tejada, González-Dugo, & Berni, 2012; Zhang, Preece, Filella, Farré-Armengol, & Peñuelas, 2017). Among these are

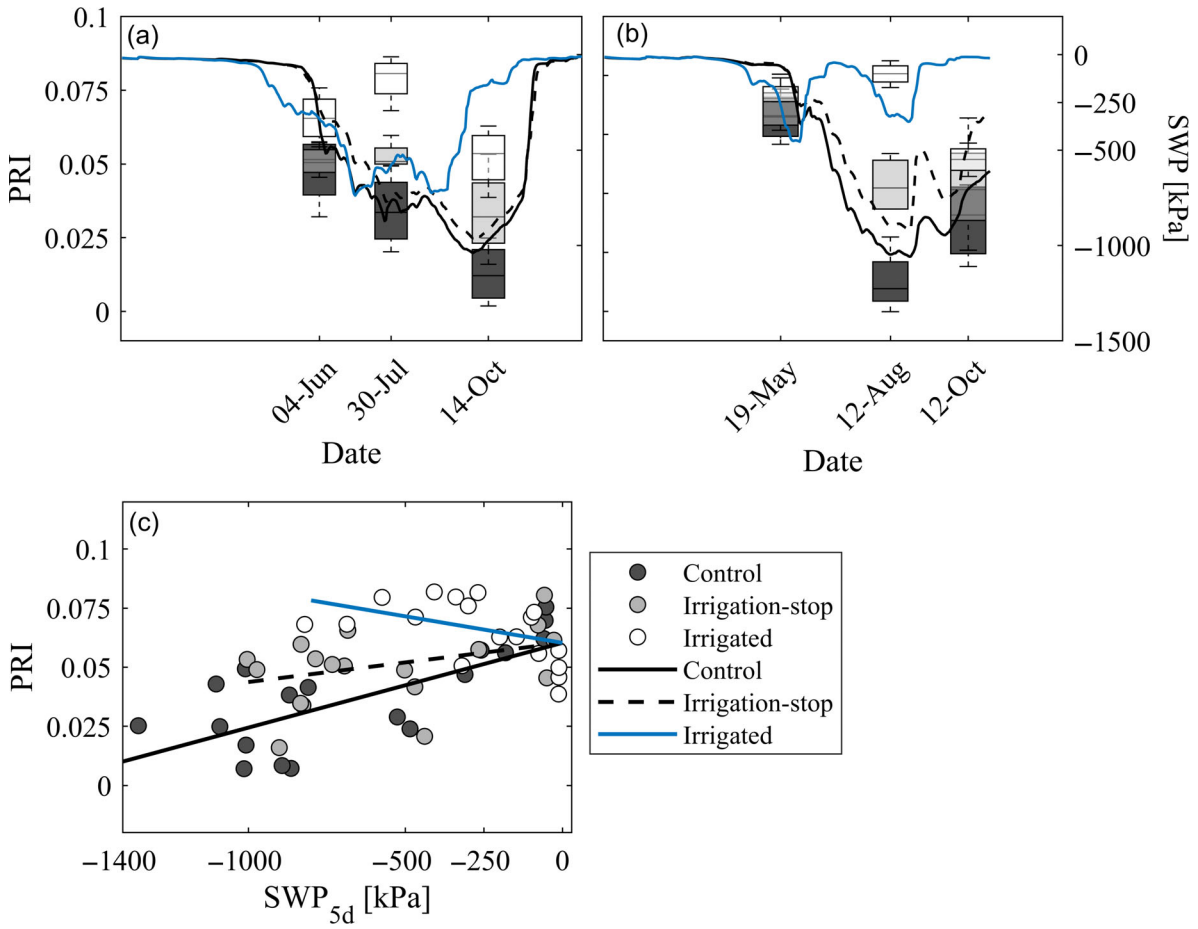

FIGURE 7 Seasonal differences in the drone-based remotely sensed photochemical reflectance index (PRI), as a function of soil water potential (SWP), at the Pfynwald *Pinus sylvestris* experimental forest site for two growing seasons. Precipitation manipulation (irrigation) treatments are represented with different shades of gray: dark for control (C), light for irrigation-stop (IS) and white for irrigated (I). (a) and (b) show PRI and SWP for C (solid black line), IS (dashed black line) and I (solid blue line) treatments, as a function of date for (a) 2019 and (b) 2020. (c) Shows (sub)plot-level PRI measurements and predictions from the linear mixed-effects model with SWP at 80 cm depth averaged over the preceding 5 days and its interaction with irrigation treatment as fixed effects and date and (sub)plots as random effects [Colour figure can be viewed at wileyonlinelibrary.com]

early studies by Zarco-Tejada and colleagues, which demonstrate the ability of airborne PRI to track seasonal and diurnal changes in stem water potential, stomatal conductance and canopy to air temperature differences in Spanish tree orchard ecosystems under different irrigation regimes (e.g., Suárez et al., 2008; Suárez et al., 2010; Zarco-Tejada et al., 2012; Zarco-Tejada et al., 2013). Studies also seem to suggest that PRI measurements can determine post-drought recovery not only in terms of water status but also in terms of photosynthetic capacity, better than other parameters commonly used to assess plant water relations, such as leaf or stem water potential. PRI has been shown to track CO_2 net assimilation rates recovering simultaneously with water status (Peguero-Pina et al., 2008) but also the impairment of photosynthetic capacity that persisted despite the recovery of water status (Sancho-Knapik, Mendoza-Herrer, Gil-Pelegrín, & Peguero-Pina, 2018). However, most of this evidence comes from short-term (e.g., 1 month or one growing season) drought experiments in seedlings or orchard ecosystems (Marino et al., 2014; Peguero-Pina et al., 2008; Sancho-Knapik et al., 2018; Zarco-Tejada et al., 2012), where the drought response is exclusively driven by concurrent environmental conditions. To the best of our knowledge, our study is the first to investigate the use of PRI to track stress and recovery in a mature natural forest in a long-term precipitation manipulation experiment, where tree responses are affected by concurrent environmental conditions, as well as functional and structural acclimation to a 17-year experimental water regime.

We found that drone-based PRI is an effective remotely sensed physiological proxy to track drought responses of *P. sylvestris* trees. Specifically, the PRI of drought-stressed control trees was up to 10 times lower than for irrigated trees, reflecting larger photoprotective pigment pool sizes and greater photoprotective non-photochemical quenching activity during summer. PRI also captured functional recovery during times of high soil water availability (SWP > −10 kPa) in spring, when photosynthesis of non-irrigated trees nearly recovered to irrigated tree levels (Figures 3d and 4d).

PRI treatment differences between control and irrigated trees during midday of summer days were larger than seasonal and diurnal variations in PRI within the same treatment, by 20% and 30%, respectively. In line with other studies (Fréchette, Chang, & Ensminger, 2016), the variation in PRI associated with seasonal

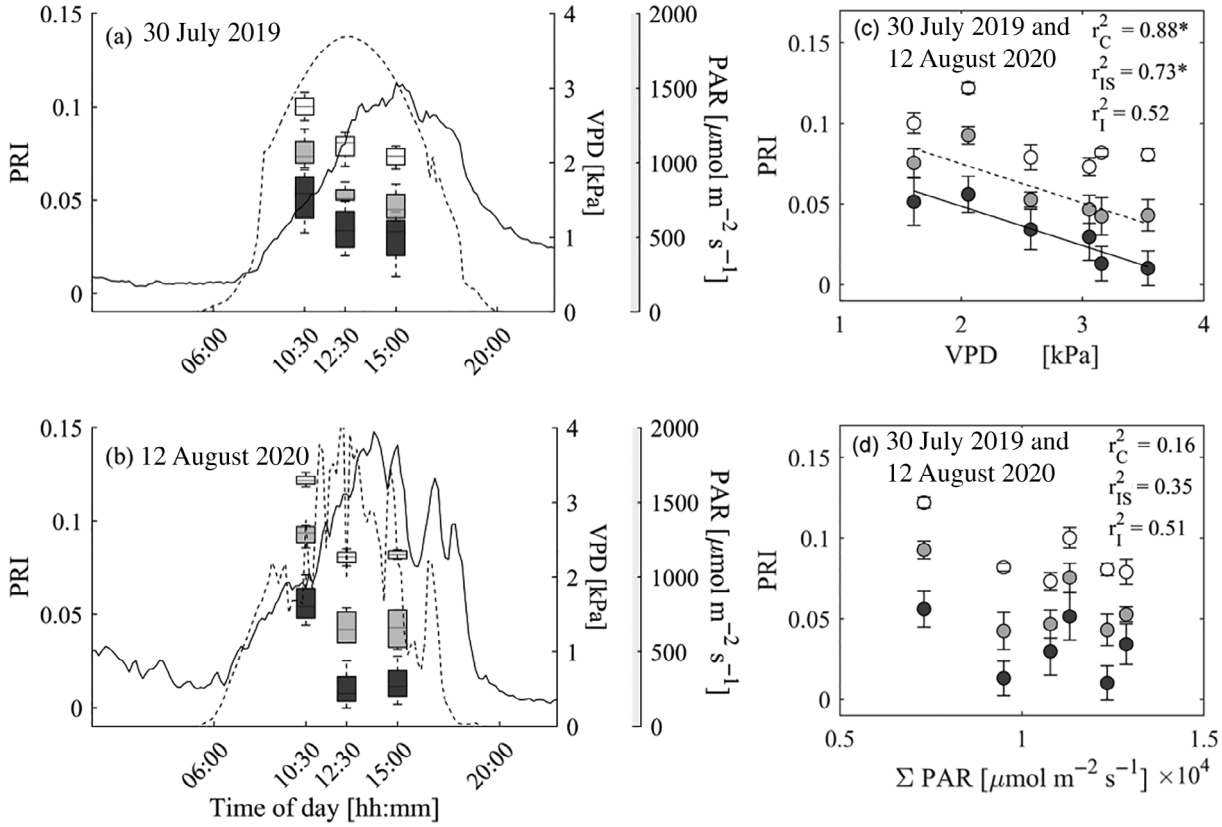

FIGURE 8 Diurnal differences in drone-based remotely sensed photochemical reflectance index (PRI), as a function of vapour pressure deficit (VPD) and photosynthetically active radiation (PAR), at the Pfynwald *Pinus sylvestris* experimental forest site for 2 days in summer. Precipitation manipulation (irrigation) treatments are represented with different shades of gray: dark for control (C), light for irrigation-stop (IS) and white for irrigated (I). (a) and (b) show PRI superimposed on VPD (solid line) and PAR (dashed line), as a function of time for (a) 30 July 2019 and (b) 12 August 2020. (c) and (d) show linear regressions of PRI versus (c) average VPD and (d) cumulated PAR, recorded over 1 hr centered around the drone flight time. Regression lines (solid = control, dashed = irrigation-stop) are included for significant correlations (*p < .05, **p < .01, ***p < .001)

changes in pigment pool sizes was larger than the variation in PRI attributable to dynamic diurnal xanthophyll cycle activity (e.g., about 10% for the control treatment). All three treatments showed comparable diurnal PRI variations, suggesting similar dynamic adjustments of xanthophyll pigments over the day. The highest PRI values (i.e., lower stress levels) occurred in the morning (~10:30 CET), when VPD < 2 kPa and PAR < 1,500 μmol m^{-2} s^{-1} (Figure 8a,b); morning PRI was lower for non-irrigated trees than for irrigated trees, reflecting a higher investment in photoprotection in the form of larger carotenoid pigment pool in these trees.

4.2 | Factors affecting the mechanistic interpretation of PRI

Past studies have shown that a series of factors can affect the variation in PRI and, under some circumstances, its sensitivity to physiological processes.

At the leaf scale, PRI is affected by a short-term rapid component linked with xanthophyll cycle activity and a long-term seasonal component related to pigment pool size adjustments, that is, Car/Chl and VAZ/Chl ratios (Wong, D'Odorico, Bhathena, Arain, & Ensminger, 2019; Wong & Gamon, 2015). These components overlap over seasonal timescales, potentially hindering a clear mechanistic interpretation of PRI (Filella et al., 2009; Gamon et al., 2016; Gamon & Berry, 2012; Sims & Gamon, 2002; Stylinski et al., 2002). This overlap has been hypothesized to be the reason for a decoupling of PRI and NPQ at seasonal time scales, with the former being controlled by seasonal adjustments in pigments pool sizes and the latter by the xanthophyll de-epoxidation status and other xanthophyll-independent mechanisms (Porcar-Castell et al., 2012). During spring recovery of photosynthetic capacity, sustained NPQ is gradually replaced by the rapidly reversible flexible energy dissipation, via the xanthophyll cycle during dehardening. Accordingly, prior to this switch PRI cannot be used to accurately detect changes in LUE (Busch, Hüner, & Ensminger, 2009), while zeaxanthin-independent mechanisms of NPQ remain in operation, decoupling the relationship between PRI and LUE (Fréchette, Wong, Junker, Chang, & Ensminger, 2015). This was confirmed in our study, as we found the strongest correlations between tree-level PRI and leaf-level pigments and physiological parameters in summer (Figures 5 and 6), while relationships between PRI and pigment parameters were especially weak

in spring (Figure 5b,f,j), confirming that PRI is unable to capture zeaxanthin-independent NPQ mechanisms.

A decoupling of PRI and NPQ was also observed in an experiment with Kermes oak (*Quercus coccifera*) seedlings during post-drought recovery, when irrigation of severely drought-stressed seedlings did not result in a drop in NPQ, while PRI captured the upregulation of photosynthetic activity (Peguero-Pina et al., 2008). In our study, PRI seemed to track the overall drop in NPQ and the upregulation of photosynthesis (Figure S3) in response to improved water availability over autumn 2020. This is also demonstrated by the strong correlations found between tree-level PRI and leaf-level DEPS and VAZ/Chl in autumn (Figure 5d,l).

PRI is a robust indicator of the leaf-level physiological processes discussed above, yet the sensitivity of PRI as a physiological proxy can be confounded at the canopy and the landscape scale by factors such as illumination conditions, viewing geometry and canopy structure (Barton & North, 2001; Hernández-Clemente et al., 2011; Hilker et al., 2008; Suárez et al., 2008). These factors could potentially influence the physiological signal during times when treatment differences are less evident, for example, during spring and autumn. Differences in illumination conditions for leaves from different canopy positions (top vs. bottom) having contrasting light histories (sun vs. shade) are known to affect leaf physiology and pigment composition and in turn PRI (Gamon & Berry, 2012). In this study, we focused on sun-exposed top-canopy leaves, which are known to invest more in photoprotection than their shaded counterparts. This was possible, thanks to a shade mask applied during the processing of drone-based imagery and to scaffolds for measuring upper canopy branches. Some authors suggest alternative PRI formulations that seem to reduce the effect of canopy structure (Hernández-Clemente et al., 2011) or enhance the sensitivity to DEPS and NPQ (Woodgate et al., 2019). All these formulations are based on the original PRI by Gamon et al. (1990, 1992), which was also chosen when customizing our multispectral sensor, which was limited to five wavelength bands for estimating PRI, CCI and NDVI. Regardless of the adopted formulation, noise in the data can be minimized through the implementation of acquisition protocols and data correction workflows (Aasen, Honkavaara, Lucieer, & Zarco-Tejada, 2018). However, complete noise removal is difficult, as shown by the year-to-year variability of physiological parameters and PRI relationships (Figure 6). Paired physiological and remotely sensed field datasets, like those collected in this study, over multiple years and a wide range of environmental conditions must be analysed to further calibrate and validate PRI-based approaches before they can be used operationally for forest stress monitoring.

4.3 | Long-term acclimation affects the current tree drought stress response

We found both concurrent environmental conditions and acclimation to past conditions resulting from the irrigation treatment to have a strong impact on *P. sylvestris* responses captured through drone-based PRI. Over seasonal timescales, we found concurrent soil water availability to be a good predictor of the PRI tree response, indicative of the trees' investment in photoprotection obtained through Car/Chl pigment pool size adjustments over the year (i.e., slow PRI component; Figure S2g–l). In line with our hypothesis, this relationship was, however, highly dependent on acclimation to past conditions. Trees in the control treatment showed the highest positive rate of change in PRI per unit of SWP, followed by irrigation-stop trees. Irrigated trees showed the lowest sensitivity to SWP changes over the growing season (Figure 7c). These results are in accordance with the sensitivity of stomatal conductance to SWP changes observed for our site (Schönbeck et al., 2021).

Over diurnal timescales, we found that atmospheric water demand (VPD) explained the large PRI tree response dynamics, indicative of photoprotective non-photochemical quenching activity (i.e., fast PRI component). All treatments showed a similar sensitivity of PRI per unit of VPD change, but treatment affected the intercept of the PRI–VPD relationship. Trees in the non-irrigated treatments started the morning with lower PRI values than trees in the irrigated treatment, and this difference was maintained throughout the day (Figure 8), suggesting a higher overall investment in photoprotection through larger carotenoid pigment pool in the non-irrigated trees.

There is substantial evidence that past conditions and derived legacy acclimation effects play an important role in explaining the degree of decoupling of plant responses from concurrent environmental conditions (Anderegg et al., 2015; Kannenberg et al., 2019; Zweifel et al., 2020). However, a full understanding of the impact over different time scales and the underlying mechanisms has yet to be reached. Structural tree acclimation is among the legacy effects that have been observed at our site since the start of irrigation in 2003, occurring gradually through the adjustment of morphological and anatomical traits in response to long-term irrigation. Reported trait adjustments in irrigated trees have included increases in leaf area, needle and shoot length (Dobbertin et al., 2010; Eilmann, Dobbertin, & Rigling, 2013; Schönbeck et al., 2018) and fine-root biomass (Brunner, Herzog, Galiano, & Gessler, 2019). Zweifel et al. (2020) conducted a study at the same site to specifically look at the acclimation of trees in the irrigation-stop treatment. The authors found different traits to have different acclimation response times, with biophysical processes responding within days, while needle and shoot length and radial stem growth started to reach control levels only after 4 years.

In this study, we found irrigation-stop trees to have intermediate and significantly different ($p \leq .05$) PRI tree responses in summer (Figure 4) and over diurnal timescales (Figure 8) compared with trees exposed to the other two treatments. This suggests that even 5–6 years after irrigation was cut off, a positive legacy effect – where trait values remained above the level of the control for several years – might still have influenced stress responses to some extent and, consequently, the photoprotective needs of these trees. Other physiological and structural traits also suggest that the acclimation of irrigation-stop trees was ongoing. For instance, leaf-level gas exchange measurements for the trees around the scaffolds suggest that irrigation-stop trees tended to have higher photosynthesis and stomatal conductance levels than control trees, although these

differences were only marginally significant in summer 2020 ($p \leq .1$; Figure S3e,k). In contrast, NPQ values were not significantly different between these two treatments (Figure S3cc). At the canopy scale, visual crown transparency estimates conducted every summer at the site based on the guidelines of the International Co-operative Programme on Assessment and Monitoring of Air Pollution Effects on Forests (ICP) (Dobbertin & Brang, 2001) confirmed the positive legacy effect. Specifically, in 2020 irrigation-stop trees had still not increased in crown transparency to the level of control trees (Figure S4), indicating an overall better health status of irrigation-stop trees than control trees.

The underlying mechanisms for such prolonged acclimation processes in irrigation-stop trees are still not fully understood and are somewhat counterintuitive. One might assume that the persistent larger leaf area and canopy size of these trees would increase drought stress and photoprotection even beyond control levels. In fact, right after irrigation was stopped at the end of 2013, trees in irrigation-stop subplots dried out the soil more severely than trees in control subplots, due to their larger crowns and higher fine-root biomass in the topsoil (data not shown). In the years that followed, however, irrigation-stop trees adjusted their aboveground traits to the new conditions (e.g., by growing shorter needles) faster than changes to their fine-root system (Brunner et al., 2019; Zweifel et al., 2020), which might partially explain the relatively low stress level observed for these trees. The potential tapping of deep roots from irrigation-stop trees into irrigated soil did not significantly influence tree responses, as shown by performing the analysis both with and without a 5 m buffer zone separating irrigation-stop and irrigated subplots (Figure S5). Although a study by Gao et al. (2021) at our same site showed that tree rhizospheres extend laterally up to 2.8 times the reach of tree canopies, our findings (Figure S5) suggest that the largest contribution to water uptake comes from fine roots in the topsoil close to the base of the tree. Water run-off from irrigated to irrigation-stop subplots is unlikely because the latter are located upslope. Further, belowground lateral water flow can be excluded because matric potentials are low, preventing mobility of the soil water. The slightly higher SWP of irrigation-stop subplots compared with control plots (Figure 1) could instead be explained by improved soil shading due to lower crown transparency (Figure S4) and fewer stand openings due to fewer dead trees (Figure 2), overriding the effect of higher transpiration by larger crowns.

Overall, this study corroborates the importance of including information on past environmental conditions and on the speed of acclimation of different traits to understand the (de)coupling of plant responses from concurrent environmental conditions and to improve the representation of these processes in vegetation models (Zhou et al., 2019).

5 | CONCLUSIONS

In this study, the high sensitivity of drone-based PRI to tree water status and photosynthetic activity made it possible to capture differences in diurnal and seasonal tree responses to environmental parameters describing atmospheric and soil drought in a mature *P. sylvestris* forest. Long-term acclimation to a 17-year precipitation manipulation (irrigation) experimental treatment influenced the seasonal relationship between tree PRI responses and water availability, demonstrating the importance of past environmental conditions in determining trees' current drought stress responses.

Most existing knowledge on drought stress physiology is based on small seedlings in short-term experiments. It might be misleading to extrapolate these findings to mature trees, as they do not represent the true responses of mature forests that have undergone acclimation. Our study demonstrates that high-throughput drone-based physiological phenotyping based on PRI can scale tree physiological responses to entire tree populations and reduce measurement time, from several days needed for classical physiological assessments to less than an hour to complete a full scan of an entire forest stand. Long-term field manipulation experiments such as the one in Pfynwald are rare (Knapp et al., 2017); nevertheless, such experiments are crucial to understand the potential of functional and structural acclimation required to alleviate the impact of drought on stomatal conductance and photosynthesis at different time scales and in turn to better predict tree responses to future warmer and drier conditions.

ACKNOWLEDGMENTS

This work was supported by the Swiss National Science Foundation (SNSF) Spark funding scheme for innovative research granted to Petra D'Odorico (CRSK-3_190802) and by an SNSF grant to Arthur Gessler (310030_189109). Ingo Ensminger acknowledges support for the drone-based phenotyping platform through a Genome Ontario PBDF grant and the Genome Canada LSARP project SpruceUp, through a National Science and Engineering Council (NSERC) grant (RGPIN-2020-06928) and through a WSL visiting fellowship. Petra D'Odorico further acknowledges the initial travel fellowship provided by the University of Toronto Mississauga. We are thankful to Chris Wong for completing the analysis and quantification of pigments and to Mauro Marty and Ruedi Bösch for field support. We are further grateful to Yann Vitasse for constructive discussions. Two anonymous reviewers provided valuable comments.

CONFLICT OF INTEREST

The authors declare no conflict of interest.

AUTHORS' CONTRIBUTIONS

Ingo Ensminger, Arthur Gessler and Petra D'Odorico conceived the study and designed the experiment. Petra D'Odorico, Leonie Schönbeck and Valentina Vitali performed field measurements with the support of the other authors. Katrin Meusburger and Roman Zweifel were responsible for continuous soil and meteorological data acquisition and Jonas Gisler for site maintenance. Vera Marjorie Elauria Velasco ran the HPLC analysis. Petra D'Odorico analysed the data and led the writing of the manuscript with important contributions from all authors.

DATA AVAILABILITY STATEMENT

The data that support the findings of this study are available from the corresponding author upon request.

ORCID

Petra D'Odorico https://orcid.org/0000-0001-9954-8508
Leonie Schönbeck https://orcid.org/0000-0001-9576-254X
Valentina Vitali https://orcid.org/0000-0002-3045-6178
Roman Zweifel https://orcid.org/0000-0001-9438-0582

REFERENCES

Aasen, H., Honkavaara, E., Lucieer, A., & Zarco-Tejada, J. P. (2018). Quantitative remote sensing at ultra-high resolution with UAV spectroscopy: A review of sensor technology, measurement procedures, and data correction workflows. *Remote Sensing*, *10*(7), 1091.

Anderegg, W. R. L., Schwalm, C., Biondi, F., Camarero, J. J., Koch, G., Litvak, M., … Pacala, S. (2015). Pervasive drought legacies in forest ecosystems and their implications for carbon cycle models. *Science*, *349*(6247), 528–532.

Barton, C. V. M., & North, P. R. J. (2001). Remote sensing of canopy light use efficiency using the photochemical reflectance index: Model and sensitivity analysis. *Remote Sensing of Environment*, *78*(3), 264–273.

Bigler, C., Bräker, O. U., Bugmann, H., Dobbertin, M., & Rigling, A. (2006). Drought as an inciting mortality factor in scots pine stands of the Valais, Switzerland. *Ecosystems*, *9*(3), 330–343.

Brunner, I., Herzog, C., Galiano, L., & Gessler, A. (2019). Plasticity of fine-root traits under long-term irrigation of a water-limited scots pine forest. *Frontiers in Plant Science*, *10*, 701. https://doi.org/10.3389/fpls.2019.00701

Brunner, I., Pannatier, E. G., Frey, B., Rigling, A., Landolt, W., Zimmermann, S., & Dobbertin, M. (2009). Morphological and physiological responses of scots pine fine roots to water supply in a dry climatic region in Switzerland. *Tree Physiology*, *29*(4), 541–550.

Busch, F., Hüner, N. P. A., & Ensminger, I. (2009). Biochemical constrains limit the potential of the photochemical reflectance index as a predictor of effective quantum efficiency of photosynthesis during the winter spring transition in Jack pine seedlings. *Functional Plant Biology*, *36*(11), 1016–1026.

Bussotti, F., Pollastrini, M., Holland, V., & Brüggemann, W. (2015). Functional traits and adaptive capacity of European forests to climate change. *Environmental and Experimental Botany*, *111*, 91–113.

Chauvier, Y., Thuiller, W., Brun, P., Lavergne, S., Descombes, P., Karger, D. N., … Zimmermann, N. E. (2020). Influence of climate, soil, and land cover on plant species distribution in the European Alps. *Ecological Monographs*, *91*(2), e01433.

D'Odorico, P., Besik, A., Wong, C. Y. S., Isabel, N., & Ensminger, I. (2020). High-throughput drone-based remote sensing reliably tracks phenology in thousands of conifer seedlings. *New Phytologist*, *226*(6), 1667–1681.

Dai, A. (2013). Increasing drought under global warming in observations and models. *Nature Climate Change*, *3*(1), 52–58.

De Boeck, H. J., & Verbeeck, H. (2011). Drought-associated changes in climate and their relevance for ecosystem experiments and models. *Biogeosciences*, *8*(5), 1121–1130.

Demmig, B., Winter, K., Krüger, A., & Czygan, F.-C. (1988). Zeaxanthin and the heat dissipation of excess light energy in *Nerium oleander* exposed to a combination of high light and water stress. *Plant Physiology*, *87*(1), 17–24.

Demmig-Adams, B. (1998). Survey of thermal energy dissipation and pigment composition in sun and shade leaves. *Plant and Cell Physiology*, *39*(5), 474–482.

Demmig-Adams, B., & Adams, W. W., III. (2006). Photoprotection in an ecological context: The remarkable complexity of thermal energy dissipation. *New Phytologist*, *172*(1), 11–21.

Demmig-Adams, B., & Adams, W. W. (1993). The xanthophyll cycle. In R. G. Alscher & J. L. Hess (Eds.), *Antioxidants in higher plants* (pp. 92–107). Boca Raton, FL: CRC Press.

Demmig-Adams, B., & Adams, W. W. (1996). The role of xanthophyll cycle carotenoids in the protection of photosynthesis. *Trends in Plant Science*, *1*(1), 21–26.

Dobbertin, M., & Brang, P. (2001). Crown defoliation improves tree mortality models. *Forest Ecology and Management*, *141*(3), 271–284.

Dobbertin, M., Eilmann, B., Bleuler, P., Giuggiola, A., Graf Pannatier, E., Landolt, W., … Rigling, A. (2010). Effect of irrigation on needle morphology, shoot and stem growth in a drought-exposed *Pinus sylvestris* forest. *Tree Physiology*, *30*(3), 346–360.

Dorado-Liñán, I., Piovesan, G., Martínez-Sancho, E., Gea-Izquierdo, G., Zang, C., Cañellas, I., … Menzel, A. (2019). Geographical adaptation prevails over species-specific determinism in trees' vulnerability to climate change at Mediterranean rear-edge forests. *Global Change Biology*, *25*(4), 1296–1314.

Eilmann, B., Dobbertin, M., & Rigling, A. (2013). Growth response of scots pine with different crown transparency status to drought release. *Annals of Forest Science*, *70*(7), 685–693.

Filella, I., Porcar-Castell, A., Munné-Bosch, S., Bäck, J., Garbulsky, M. F., & Peñuelas, J. (2009). PRI assessment of long-term changes in carotenoids/chlorophyll ratio and short-term changes in de-epoxidation state of the xanthophyll cycle. *International Journal of Remote Sensing*, *30*(17), 4443–4455.

Flexas, J., & Medrano, H. (2002). Energy dissipation in C3 plants under drought. *Functional Plant Biology*, *29*(10), 1209–1215.

Fréchette, E., Chang, C. Y.-Y., & Ensminger, I. (2016). Photoperiod and temperature constraints on the relationship between the photochemical reflectance index and the light use efficiency of photosynthesis in *Pinus strobus*. *Tree Physiology*, *36*(3), 311–324.

Fréchette, E., Wong, C. Y. S., Junker, L. V., Chang, C. Y.-Y., & Ensminger, I. (2015). Zeaxanthin-independent energy quenching and alternative electron sinks cause a decoupling of the relationship between the photochemical reflectance index (PRI) and photosynthesis in an evergreen conifer during spring. *Journal of Experimental Botany*, *66*(22), 7309–7323.

Gamon, J. A., & Berry, J. A. (2012). Facultative and constitutive pigment effects on the photochemical reflectance index (PRI) in sun and shade conifer needles. *Israel Journal of Plant Sciences*, *60*(1–2), 85–95.

Gamon, J. A., Field, C. B., Bilger, W., Björkman, O., Fredeen, A. L., & Peñuelas, J. (1990). Remote sensing of the xanthophyll cycle and chlorophyll fluorescence in sunflower leaves and canopies. *Oecologia*, *85*(1), 1–7.

Gamon, J. A., Huemmrich, K. F., Wong, C. Y. S., Ensminger, I., Garrity, S., Hollinger, D. Y., … Peñuelas, J. (2016). A remotely sensed pigment index reveals photosynthetic phenology in evergreen conifers. *Proceedings of the National Academy of Sciences*, *113*(46), 13087–13092.

Gamon, J. A., Peñuelas, J., & Field, C. B. (1992). A narrow-waveband spectral index that tracks diurnal changes in photosynthetic efficiency. *Remote Sensing of Environment*, *41*(1), 35–44.

Gamon, J. A., Serrano, L., & Surfus, J. S. (1997). The photochemical reflectance index: An optical indicator of photosynthetic radiation use efficiency across species, functional types, and nutrient levels. *Oecologia*, *112*(4), 492–501.

Gao, D., Joseph, J., Werner, R. A., Brunner, I., Zürcher, A., Hug, C., … Hagedorn, F. (2021). Drought alters the carbon footprint of trees in soils—Tracking the spatio-temporal fate of 13C-labelled assimilates in the soil of an old-growth pine forest. *Global Change Biology*, *27*(11), 2491–2506.

Garbulsky, M. F., Peñuelas, J., Gamon, J., Inoue, Y., & Filella, I. (2011). The photochemical reflectance index (PRI) and the remote sensing of leaf, canopy and ecosystem radiation use efficiencies: A review and meta-analysis. *Remote Sensing of Environment*, *115*(2), 281–297.

Genty, B., Briantais, J.-M., & Baker, N. R. (1989). The relationship between the quantum yield of photosynthetic electron transport and quenching

of chlorophyll fluorescence. *Biochimica et Biophysica Acta (BBA) - General Subjects*, *990*(1), 87–92.

Gessler, A., Bottero, A., Marshall, J., & Arend, M. (2020). The way back: Recovery of trees from drought and its implication for acclimation. *New Phytologist*, *228*(6), 1704–1709.

Goerner, A., Reichstein, M., & Rambal, S. (2009). Tracking seasonal drought effects on ecosystem light use efficiency with satellite-based PRI in a Mediterranean forest. *Remote Sensing of Environment*, *113*(5), 1101–1111.

Hernández-Clemente, R., Navarro-Cerrillo, R. M., Suárez, L., Morales, F., & Zarco-Tejada, P. J. (2011). Assessing structural effects on PRI for stress detection in conifer forests. *Remote Sensing of Environment*, *115*(9), 2360–2375.

Hilker, T., Coops, N. C., Hall, F. G., Black, T. A., Wulder, M. A., Nesic, Z., & Krishnan, P. (2008). Separating physiologically and directionally induced changes in PRI using BRDF models. *Remote Sensing of Environment*, *112*(6), 2777–2788.

Jahns, P., & Holzwarth, A. R. (2012). The role of the xanthophyll cycle and of lutein in photoprotection of photosystem II. *Biochimica et Biophysica Acta (BBA) - Bioenergetics*, *1817*(1), 182–193.

Junker, L. V., & Ensminger, I. (2016). Fast detection of leaf pigments and isoprenoids for ecophysiological studies, plant phenotyping and validating remote-sensing of vegetation. *Physiologia Plantarum*, *158*(4), 369–381.

Kannenberg, S. A., Maxwell, J. T., Pederson, N., D'Orangeville, L., Ficklin, D. L., & Phillips, R. P. (2019). Drought legacies are dependent on water table depth, wood anatomy and drought timing across the eastern US. *Ecology Letters*, *22*(1), 119–127.

Knapp, A. K., Avolio, M. L., Beier, C., Carroll, C. J. W., Collins, S. L., Dukes, J. S., … Smith, M. D. (2017). Pushing precipitation to the extremes in distributed experiments: Recommendations for simulating wet and dry years. *Global Change Biology*, *23*(5), 1774–1782.

Kremer, A., Potts, B. M., & Delzon, S. (2014). Genetic divergence in forest trees: Understanding the consequences of climate change. *Functional Ecology*, *28*(1), 22–36.

Marino, G., Pallozzi, E., Cocozza, C., Tognetti, R., Giovannelli, A., Cantini, C., & Centritto, M. (2014). Assessing gas exchange, sap flow and water relations using tree canopy spectral reflectance indices in irrigated and rainfed *Olea europaea* L. *Environmental and Experimental Botany*, *99*, 43–52.

Nicotra, A. B., Atkin, O. K., Bonser, S. P., Davidson, A. M., Finnegan, E. J., Mathesius, U., … van Kleunen, M. (2010). Plant phenotypic plasticity in a changing climate. *Trends in Plant Science*, *15*(12), 684–692.

Niyogi, K. K. (1999). Photoprotection revisited: Genetic and molecular approaches. *Annual Review of Plant Physiology and Plant Molecular Biology*, *50*(1), 333–359.

Otsu, K., Pla, M., Duane, A., Cardil, A., & Brotons, L. (2019). Estimating the threshold of detection on tree crown defoliation using vegetation indices from UAS multispectral imagery. *Drones*, *3*(4), 80.

Peguero-Pina, J. J., Morales, F., Flexas, J., Gil-Pelegrín, E., & Moya, I. (2008). Photochemistry, remotely sensed physiological reflectance index and de-epoxidation state of the xanthophyll cycle in Quercus coccifera under intense drought. *Oecologia*, *156*, 1–11.

Peñuelas, J., Filella, I., & Gamon, J. A. (1995). Assessment of photosynthetic radiation-use efficiency with spectral reflectance. *New Phytologist*, *131*(3), 291–296.

Peñuelas, J., Munné-Bosch, S., Llusià, J., & Filella, I. (2004). Leaf reflectance and photo- and antioxidant protection in field-grown summer-stressed Phillyrea angustifolia. Optical signals of oxidative stress? *New Phytologist*, *162*(1), 115–124.

Porcar-Castell, A., Garcia-Plazaola, J. I., Nichol, C. J., Kolari, P., Olascoaga, B., Kuusinen, N., … Nikinmaa, E. (2012). Physiology of the seasonal relationship between photochemical reflectance index and photosynthetic light use efficiency. *Oecologia*, *170*, 313–323.

Ramírez-Valiente, J. A., Solé-Medina, A., Pyhäjärvi, T., Savolainen, O., Cervantes, S., Kesälahti, R., … Robledo-Arnuncio, J. J. (2021). Selection patterns on early-life phenotypic traits in *Pinus sylvestris* are associated with precipitation and temperature along a climatic gradient in Europe. *New Phytologist*, *229*(5), 3009–3025.

Rebetez, M., & Dobbertin, M. (2004). Climate change may already threaten scots pine stands in the Swiss Alps. *Theoretical and Applied Climatology*, *79*(1), 1–9.

Richardson, D. M. (1998). *Ecology and biogeography of Pinus* (p. 527). New York, NY: Cambridge University Press.

Rigling, A., Bigler, C., Eilmann, B., Feldmeyer-Christe, E., Gimmi, U., Ginzler, C., … Dobbertin, M. (2013). Driving factors of a vegetation shift from scots pine to pubescent oak in dry alpine forests. *Global Change Biology*, *19*(1), 229–240.

Sancho-Knapik, D., Mendoza-Herrer, Ó., Gil-Pelegrín, E., & Peguero-Pina, J. J. (2018). Chl fluorescence parameters and leaf reflectance indices allow monitoring changes in the physiological status of *Quercus ilex* L. under progressive water deficit. *Forests*, *9*(7), 400.

Schleppi, P. (2018). Pixstat 1.2.0.0. Retrieved July 7, 2019 from http://www.wsl.ch/dienstleistungenprodukte/software/pixstat

Schönbeck, L., Gessler, A., Hoch, G., McDowell, N. G., Rigling, A., Schaub, M., & Li, M.-H. (2018). Homeostatic levels of nonstructural carbohydrates after 13 yr of drought and irrigation in *Pinus sylvestris*. *New Phytologist*, *219*(4), 1314–1324.

Schönbeck, L., Grossiord, C., Gessler, A., Gisler, J., Meusburger, K., D'Odorico, P., … Schaub, M. (2021). Photosynthetic acclimation and sensitivity to short- and long-term environmental changes. *bioRxiv*, 2021.2001.2004.425174.

Sims, D. A., & Gamon, J. A. (2002). Relationships between leaf pigment content and spectral reflectance across a wide range of species, leaf structures and developmental stages. *Remote Sensing of Environment*, *81*(2), 337–354.

Spilke, J., Piepho, H. P., & Hu, X. (2005). Analysis of unbalanced data by mixed linear models using the mixed procedure of the SAS system. *Journal of Agronomy and Crop Science*, *191*(1), 47–54.

Stahl, U., Reu, B., & Wirth, C. (2014). Predicting species' range limits from functional traits for the tree flora of North America. *Proceedings of the National Academy of Sciences*, *111*(38), 13739–13744.

Stylinski, C., Gamon, J., & Oechel, W. (2002). Seasonal patterns of reflectance indices, carotenoid pigments and photosynthesis of evergreen chaparral species. *Oecologia*, *131*(3), 366–374.

Suárez, L., Zarco-Tejada, P. J., González-Dugo, V., Berni, J. A. J., Sagardoy, R., Morales, F., & Fereres, E. (2010). Detecting water stress effects on fruit quality in orchards with time-series PRI airborne imagery. *Remote Sensing of Environment*, *114*(2), 286–298.

Suárez, L., Zarco-Tejada, P. J., Sepulcre-Cantó, G., Pérez-Priego, O., Miller, J. R., Jiménez-Muñoz, J. C., & Sobrino, J. (2008). Assessing canopy PRI for water stress detection with diurnal airborne imagery. *Remote Sensing of Environment*, *112*(2), 560–575.

Thayer, S. S., & Björkman, O. (1990). Leaf xanthophyll content and composition in sun and shade determined by HPLC. *Photosynthesis Research*, *23*(3), 331–343.

Thimonier, A., Graf Pannatier, E., Schmitt, M., Waldner, P., Walthert, L., Schleppi, P., … Kräuchi, N. (2010). Does exceeding the critical loads for nitrogen alter nitrate leaching, the nutrient status of trees and their crown condition at Swiss long-term forest ecosystem research (LWF) sites? *European Journal of Forest Research*, *129*(3), 443–461.

Tyrmi, J. S., Vuosku, J., Acosta, J. J., Li, Z., Sterck, L., Cervera, M. T., … Pyhäjärvi, T. (2020). Genomics of clinal local adaptation in *Pinus sylvestris* under continuous environmental and spatial genetic setting. *G3 Genes|Genomes|Genetics*, *10*(8), 2683–2696.

Walthert, L., & Schleppi, P. (2018). Equations to compensate for the temperature effect on readings from dielectric decagon MPS-2 and MPS-6 water potential sensors in soils. *Journal of Plant Nutrition and Soil Science*, *181*(5), 749–759.

Williams, P. A., Allen, C. D., Macalady, A. K., Griffin, D., Woodhouse, C. A., Meko, D. M., … McDowell, N. G. (2013). Temperature as a potent driver of regional forest drought stress and tree mortality. *Nature Climate Change*, *3*(3), 292–297.

Wong, C. Y. S., D'Odorico, P., Arain, M. A., & Ensminger, I. (2020). Tracking the phenology of photosynthesis using carotenoid-sensitive and near-infrared reflectance vegetation indices in a temperate evergreen and mixed deciduous forest. *New Phytologist*, *226*(6), 1682–1695.

Wong, C. Y. S., D'Odorico, P., Bhathena, Y., Arain, M. A., & Ensminger, I. (2019). Carotenoid based vegetation indices for accurate monitoring of the phenology of photosynthesis at the leaf-scale in deciduous and evergreen trees. *Remote Sensing of Environment*, *233*, 111407.

Wong, C. Y. S., & Gamon, J. A. (2015). Three causes of variation in the photochemical reflectance index (PRI) in evergreen conifers. *New Phytologist*, *206*(1), 187–195.

Woodgate, W., Suarez, L., van Gorsel, E., Cernusak, L. A., Dempsey, R., Devilla, R., … Norton, A. J. (2019). Tri-PRI: A three band reflectance index tracking dynamic photoprotective mechanisms in a mature eucalypt forest. *Agricultural and Forest Meteorology*, *272-273*, 187–201.

Yang, J. C., Magney, T. S., Yan, D., Knowles, J. F., Smith, W. K., Scott, R. L., & Barron-Gafford, G. A. (2020). The photochemical reflectance index (PRI) captures the ecohydrologic sensitivity of a semiarid mixed conifer forest. *Journal of Geophysical Research – Biogeosciences*, *125*(11), e2019JG005624.

Zarco-Tejada, P. J., González-Dugo, V., & Berni, J. A. J. (2012). Fluorescence, temperature and narrow-band indices acquired from a UAV platform for water stress detection using a micro-hyperspectral imager and a thermal camera. *Remote Sensing of Environment*, *117*, 322–337.

Zarco-Tejada, P. J., González-Dugo, V., Williams, L. E., Suárez, L., Berni, J. A. J., Goldhamer, D., & Fereres, E. (2013). A PRI-based water stress index combining structural and chlorophyll effects: Assessment using diurnal narrow-band airborne imagery and the CWSI thermal index. *Remote Sensing of Environment*, *138*, 38–50.

Zarco-Tejada, P. J., Morales, A., Testi, L., & Villalobos, F. J. (2013). Spatio-temporal patterns of chlorophyll fluorescence and physiological and structural indices acquired from hyperspectral imagery as compared with carbon fluxes measured with eddy covariance. *Remote Sensing of Environment*, *133*, 102–115.

Zhang, C., Preece, C., Filella, I., Farré-Armengol, G., & Peñuelas, J. (2017). Assessment of the response of photosynthetic activity of mediterranean evergreen oaks to enhanced drought stress and recovery by using PRI and R690/R630. *Forests*, *8*(10), 386.

Zhou, S.-X., Prentice, I. C., & Medlyn, B. E. (2019). Bridging drought experiment and modeling: Representing the differential sensitivities of leaf gas exchange to drought. *Frontiers in Plant Science*, *9*, 1965.

Zuur, A., Ieno, E. N., Walker, N., Saveliev, A. A., & Smith, G. M. (2009). *Mixed effects models and extensions in ecology with R* (2009th ed.). New York, NY: Springer.

Zweifel, R., Etzold, S., Sterck, F., Gessler, A., Anfodillo, T., Mencuccini, M., … Rigling, A. (2020). Determinants of legacy effects in pine trees – Implications from an irrigation-stop experiment. *New Phytologist*, *227*(4), 1081–1096.

SUPPORTING INFORMATION

Additional supporting information may be found in the online version of the article at the publisher's website.

How to cite this article: D'Odorico, P., Schönbeck, L., Vitali, V., Meusburger, K., Schaub, M., Ginzler, C., Zweifel, R., Velasco, V. M. E., Gisler, J., Gessler, A., & Ensminger, I. (2021). Drone-based physiological index reveals long-term acclimation and drought stress responses in trees. *Plant, Cell & Environment*, 1–19. https://doi.org/10.1111/pce.14177